References

1. Aruga J, Mikoshiba K (2003) Identification and characterization of Slitrk, a novel neuronal transmembrane protein family controlling neurite outgrowth. Mol Cell Neurosci 24: 117–129.
2. Aruga J, Yokota N, Mikoshiba K (2003) Human SLITRK family genes: genomic organization and expression profiling in normal brain and brain tumor tissue. Gene 315: 87–94.
3. Patapoutian A, Reichardt LF (2001) Trk receptors: mediators of neurotrophin action. Curr Opin Neurobiol 11: 272–280.
4. Aruga J (2003) Slitrk6 expression profile in the mouse embryo and its relationship to that of Nlrr3. Gene Expr Patterns 3: 727–733.
5. Katayama K, Zine A, Ota M, Matsumoto Y, Inoue T, et al. (2009) Disorganized innervation and neuronal loss in the inner ear of Slitrk6-deficient mice. PLoS One 4: e7786.
6. Stillman AA, Krsnik Z, Sun J, Rasin MR, State MW, et al. (2009) Developmentally regulated and evolutionarily conserved expression of SLITRK1 in brain circuits implicated in Tourette syndrome. J Comp Neurol 513: 21–37.
7. Abelson JF, Kwan KY, O'Roak BJ, Baek DY, Stillman AA, et al. (2005) Sequence variants in SLITRK1 are associated with Tourette's syndrome. Science 310: 317–320.
8. Shmelkov SV, Hormigo A, Jing D, Proenca CC, Bath KG, et al. (2010) Slitrk5 deficiency impairs corticostriatal circuitry and leads to obsessive-compulsive-like behaviors in mice. Nat Med 16: 598–602.
9. Piton A, Gauthier J, Hamdan FF, Lafreniere RG, Yang Y, et al. Systematic resequencing of X-chromosome synaptic genes in autism spectrum disorder and schizophrenia. Mol Psychiatry. In press.
10. Smith EN, Bloss CS, Badner JA, Barrett T, Belmonte PL, et al. (2009) Genome-wide association study of bipolar disorder in European American and African American individuals. Mol Psychiatry 14: 755–763.
11. Zuchner S, Cuccaro ML, Tran-Viet KN, Cope H, Krishnan RR, et al. (2006) SLITRK1 mutations in trichotillomania. Mol Psychiatry 11: 887–889.
12. Miranda DM, Wigg K, Kabia EM, Feng Y, Sandor P, et al. (2009) Association of SLITRK1 to Gilles de la Tourette syndrome. Am J Med Genet B Neuropsychiatr Genet 150B: 483–486.
13. Katayama K, Yamada K, Ornthanalai VG, Inoue T, Ota M, et al. (2010) Slitrk1-deficient mice display elevated anxiety-like behavior and noradrenergic abnormalities. Mol Psychiatry 15: 177–184.
14. Willott JF (2006) Overview of methods for assessing the mouse auditory system. Curr Protoc Neurosci Chapter 8: Unit8 21A.
15. Hardisty-Hughes RE, Parker A, Brown SD (2010) A hearing and vestibular phenotyping pipeline to identify mouse mutants with hearing impairment. Nat Protoc 5: 177–190.
16. Zhou X, Jen PH, Seburn KL, Frankel WN, Zheng QY (2006) Auditory brainstem responses in 10 inbred strains of mice. Brain Res 1091: 16–26.
17. Friedman LM, Dror AA, Avraham KB (2007) Mouse models to study inner ear development and hereditary hearing loss. Int J Dev Biol 51: 609–631.
18. Leibovici M, Safieddine S, Petit C (2008) Mouse models for human hereditary deafness. Curr Top Dev Biol 84: 385–429.
19. Bonsch D, Schmidt CM, Scheer P, Bohlender J, Neumann C, et al. (2009) A new gene locus for an autosomal-dominant non-syndromic hearing impairment (DFNA 33) is situated on chromosome 13q34-qter. (German) HNO 57: 371–376.
20. Carnicero E, Knipper M, Tan J, Alonso MT, Schimmang T (2002) Herpes simplex virus type 1-mediated transfer of neurotrophin-3 stimulates survival of chicken auditory sensory neurons. Neurosci Lett 321: 149–152.
21. Noushi F, Richardson RT, Hardman J, Clark G, O'Leary S (2005) Delivery of neurotrophin-3 to the cochlea using alginate beads. Otol Neurotol 26: 528–533.
22. Staecker H, Kopke R, Malgrange B, Lefebvre P, Van de Water TR (1996) NT-3 and/or BDNF therapy prevents loss of auditory neurons following loss of hair cells. Neuroreport 7: 889–894.
23. Calabrese DR, Hullar TE (2006) Planar relationships of the semicircular canals in two strains of mice. J Assoc Res Otolaryngol 7: 151–159.
24. Salvinelli F, Firrisi L, Casale M, Trivelli M, D'Ascanio L, et al. (2004) Benign paroxysmal positional vertigo: diagnosis and treatment. Clin Ter 155: 395–400.
25. Korres SG, Balatsouras DG, Papouliakos S, Ferekidis E (2007) Benign paroxysmal positional vertigo and its management. Med Sci Monit 13: CR275–282.
26. O'Reilly RC, Morlet T, Nicholas BD, Josephson G, Horlbeck D, et al. Prevalence of vestibular and balance disorders in children. Otol Neurotol. In press.
27. Wiener-Vacher SR (2008) Vestibular disorders in children. Int J Audiol 47: 578–583.
28. Butler AB (1995) The dorsal thalamus of jawed vertebrates: a comparative viewpoint. Brain Behav Evol 46: 209–223.
29. Nunez A, Malmierca E (2007) Corticofugal modulation of sensory information. Adv Anat Embryol Cell Biol 187: 1–74.
30. Alitto HJ, Usrey WM (2003) Corticothalamic feedback and sensory processing. Curr Opin Neurobiol 13: 440–445.
31. Katoh A, Kitazawa H, Itohara S, Nagao S (1998) Dynamic characteristics and adaptability of mouse vestibulo-ocular and optokinetic response eye movements and the role of the flocculo-olivary system revealed by chemical lesions. Proc Natl Acad Sci USA 95: 7705–7710.
32. Shutoh F, Ohki M, Kitazawa H, Itohara S, Nagao S (2006) Memory trace of motor learning shifts transsynaptically from cerebellar cortex to nuclei for consolidation. Neuroscience 139: 767–777.
33. Harrod CG, Baker JF (2003) The vestibulo ocular reflex (VOR) in otoconia deficient head tilt (het) mutant mice versus wild type C57BL/6 mice. Brain Res 972: 75–83.
34. Jastreboff PW (1979) Evaluation and statistical judgment of neural responses to sinusoidal stimulation in cases with superimposed drift and noise. Biol Cybern 33: 113–120.
35. Sakatani S, Yamada K, Homma C, Munesue S, Yamamoto Y, et al. (2009) Deletion of RAGE causes hyperactivity and increased sensitivity to auditory stimuli in mice. PLoS One 4: e8309.

LETTER

doi:10.1038/nature09544

L1 retrotransposition in neurons is modulated by MeCP2

Alysson R. Muotri[1]*, Maria C. N. Marchetto[2]*, Nicole G. Coufal[2], Ruth Oefner[2], Gene Yeo[3], Kinichi Nakashima[4] & Fred H. Gage[2]

Long interspersed nuclear elements-1 (LINE-1 or L1s) are abundant retrotransposons that comprise approximately 20% of mammalian genomes[1–3]. Active L1 retrotransposons can impact the genome in a variety of ways, creating insertions, deletions, new splice sites or gene expression fine-tuning[4–6]. We have shown previously that L1 retrotransposons are capable of mobilization in neuronal progenitor cells from rodents and humans and evidence of massive L1 insertions was observed in adult brain tissues but not in other somatic tissues[7,8]. In addition, L1 mobility in the adult hippocampus can also be influenced by the environment[9]. The neuronal specificity of somatic L1 retrotransposition in neural progenitors is partially due to the transition of a Sox2/HDAC1 repressor complex to a Wnt-mediated T-cell factor/lymphoid enhancer factor (TCF/LEF) transcriptional activation[7,10]. The transcriptional switch accompanies chromatin remodelling during neuronal differentiation, allowing a transient stimulation of L1 transcription[7]. The activity of L1 retrotransposons during brain development can have an impact on gene expression and neuronal function, thereby increasing brain-specific genetic mosaicism[11,12]. Further understanding of the molecular mechanisms that regulate L1 expression should provide new insights into the role of L1 retrotransposition during brain development. Here we show that L1 neuronal transcription and retrotransposition in rodents is increased in the absence of methyl-CpG-binding protein 2 (MeCP2), a protein involved in global DNA methylation and human neurodevelopmental diseases. Using neuronal progenitor cells derived from human induced pluripotent stem cells and human tissues, we revealed that patients with Rett syndrome (RTT), carrying MeCP2 mutations, have increased susceptibility for L1 retrotransposition. Our data demonstrate that L1 retrotransposition can be controlled in a tissue-specific manner and that disease-related genetic mutations can influence the frequency of neuronal L1 retrotransposition. Our findings add a new level of complexity to the molecular events that can lead to neurological disorders.

In neural stem cells, the repressor complex on the L1 promoter region (L1 5′UTR) includes the transcriptional factor Sox2 and the histone deacetylase 1 protein (HDAC1)[7], a MeCP2 partner[13,14]. MeCP2 has been shown to interfere with the L1 5′UTR promoter activity in transformed cell lines[15]. To investigate the role of MeCP2 in the activity of L1 promoter in neural stem cells, we cloned the L1 promoter region upstream to the luciferase gene, generating the L1 5′UTR–Luc plasmid[7]. Methylation of the L1 5′UTR–Luc reduced the promoter activity in neural stem cells (Fig. 1a and Supplementary Fig. 1a). Reduction of MeCP2 levels using siRNAs led to an increase in luciferase activity (Fig. 1b and Supplementary Fig. 1b). Transfection of the L1 5′UTR–Luc methylated plasmid in mouse neuroepithelial cells revealed that the L1 promoter activity was approximately four times more active in the MeCP2 knockout (KO) background than in wild-type (Fig. 1c and Supplementary Fig. 1c). Ectopic MeCP2 expression reduced the luciferase activity in MeCP2 KO cells close to wild-type levels (Fig. 1c).

We repeated the luciferase assay using neuroepithelial cells from a sibling MBD1 KO animal[16]. MBD1 (methyl-binding protein 1) is part of the methyl-binding protein family and has differential DNA specificity

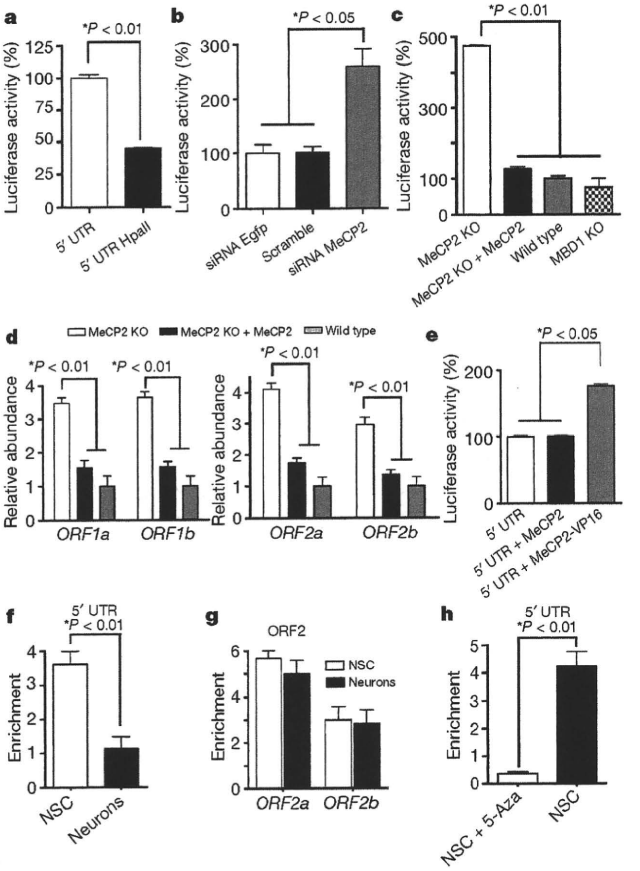

Figure 1 | MeCP2 silences L1 expression. **a**, Methylation of the L1 5′UTR–Luc reduced its transcriptional activity. **b**, Reduction of MeCP2 transcripts correlates with increased L1 promoter activity. **c**, Increased L1 promoter activity in the absence of MeCP2 but not MBD1. **d**, L1 RNA levels correlate with MeCP2 expression. **e**, Expression of the MeCP2-VP16 increased the activity of the L1 5′UTR promoter. **f**, **g**, Recruitment of MeCP2 on L1 sequences by ChIP in neural stem cells (NSC) or neurons, using 5′UTR primers (**f**) and two ORF2 regions (**g**). **h**, Occupancy of MeCP2 on the L1 promoter requires DNA methylation. Removal of DNA methylation with 5-azacytidine (5-Aza) reduced MeCP2 association to L1 promoter. ChIP-qPCR shows enrichment over IgG control precipitation. All experiments show experimental triplicates. Error bars in all panels show s.e.m.

[1]University of California San Diego, School of Medicine, Department of Pediatrics/Rady Children's Hospital San Diego, Department of Cellular & Molecular Medicine, Stem Cell Program, 9500 Gilman Drive, La Jolla, California 92093-0695, USA. [2]Laboratory of Genetics, The Salk Institute for Biological Studies, 10010 North Torrey Pines Road, La Jolla, California 92037, USA. [3]University of California San Diego, School of Medicine, Department of Cellular & Molecular Medicine, Stem Cell Program, 9500 Gilman Dr, La Jolla, California 92093-0695, USA. [4]Laboratory of Molecular Neuroscience, Graduate School of Biological Sciences, Nara Institute of Science and Technology, 8916-5 Takayama, Ikoma 630-0101, Japan.
*These authors contributed equally to this work.

when compared to MeCP2[17]. The L1 promoter was not activated in MBD1 KO background, a finding that is consistent with the idea that L1 transcriptional repression is specific to MeCP2 (Fig. 1c). Moreover, the promoter activity correlated well with the level of L1 RNA, as measured by qPCR (Fig. 1d). Ectopic MeCP2 expression reduced L1 RNA levels in the MeCP2 KO background (Fig. 1d). We co-transfected neural stem cells with the methylated L1 5′UTR–Luc and a plasmid containing either the MeCP2 cDNA or the MeCP2 fused with the transactivator domain VP16. The overexpression of MeCP2 alone did not change the luciferase levels, but the MeCP2-VP16 fusion increased luciferase levels twofold (Fig. 1e).

Using chromatin immunoprecipitation (ChIP) followed by quantitative PCR (qPCR), we detected high levels of MeCP2 in association with endogenous L1 promoter regions in neural stem cells compared to neurons (Fig. 1f). MeCP2 was also associated with other L1 regions (ORF2), but this association did not change during differentiation (Fig. 1g; see controls for ChIP experiments in Supplementary Fig. 1d, e). After treatment with 5-azacytidine, the MeCP2 ChIP signal was reduced and L1 expression increased (Fig. 1h and Supplementary Fig. 1f). A set of the CpG sites within the L1 promoter had a tendency to demethylate during neuronal differentiation, indicating that DNA methylation may silence L1 expression in neural stem cells by attracting MeCP2 (Supplementary Fig. 1g, h).

To study L1 regulation *in vivo*, we compared the brains of the L1–EGFP (enhanced green fluorescent protein) transgenic mice in wild-type and MeCP2 KO backgrounds. L1–EGFP transgenic mice have a L1 indicator cassette that will only activate the EGFP reporter after retrotransposition[7] (Supplementary Fig. 2a). The numbers of EGFP-positive cells in the brains of MeCP2 KO mice were significantly higher than in wild type (Fig. 2a, b). EGFP-positive cells were also observed in the germ line of MeCP2 KO at similar frequency as in wild-type animals, but not in other somatic tissues (Supplementary Fig. 2b). To visualize the distribution of EGFP-positive cells, we generated high-resolution, three-dimensional maps of both MeCP2 KO and wild-type brains. Although MeCP2 KO brain sections had an average of 3.5-fold more EGFP-positive cells than wild type, certain brain structures were more prone to L1 retrotransposition (Fig. 2b, c). Specifically, the cerebellum, striatum, cortex, hippocampus and olfactory bulb contained 4.2-, 5.3-, 2.8-, 6.3- and 3.8-fold more EGFP-positive neurons, respectively, in the MeCP2 KO genetic background than in wild type (Supplementary Fig. 3 and Supplementary Movie). More EGFP-positive cells may suggest an increased rate of L1 retrotransposition and/or higher rate of MeCP2 KO cell proliferation with the newly retrotransposed EGFP reporter. We found no evidence that neuroepithelial cells from the MeCP2 KO genetic background had a higher rate of division than wild type (Supplementary Fig. 4a).

We next asked whether endogenous L1 retrotransposition was also increased in the MeCP2 KO brain. New insertions from retroelements can be quantified using a qPCR approach[8,18]. To determine the activity of endogenous L1 elements, we developed a technique based on single-cell genomic qPCR that measures the frequency of mouse L1 sequences within the genome (Fig. 3a). We proposed that MeCP2 KO-derived neuroepithelial cells would have increased genomic content of L1 sequences compared to wild-type cells. Neuroepithelial cells from wild-type and MeCP2 KO sibling mouse embryos were synchronized in G1 phase and karyotyped, to avoid interference during genomic L1 detection (Supplementary Fig. 4b, c). Finally, single-cell amplification using primers for ORF2 from active L1 families confirmed the presence of the expected amplicons (Supplementary Fig. 4d). MeCP2 KO-derived neuroepithelial cells displayed significantly more ORF2 genomic copies than wild-type cells (Fig. 3b). Specific primers for the L1 5′UTR were also tested in neuroepithelial cells and did not reveal an increase in copy number in MeCP2 KO background (Fig. 3c). This lack of difference can be explained by the fact that, upon retrotransposition, the 5′ region of the L1 sequence is frequently truncated[19,20]. Also, no difference between genetic backgrounds was observed when using primers for non-mobile

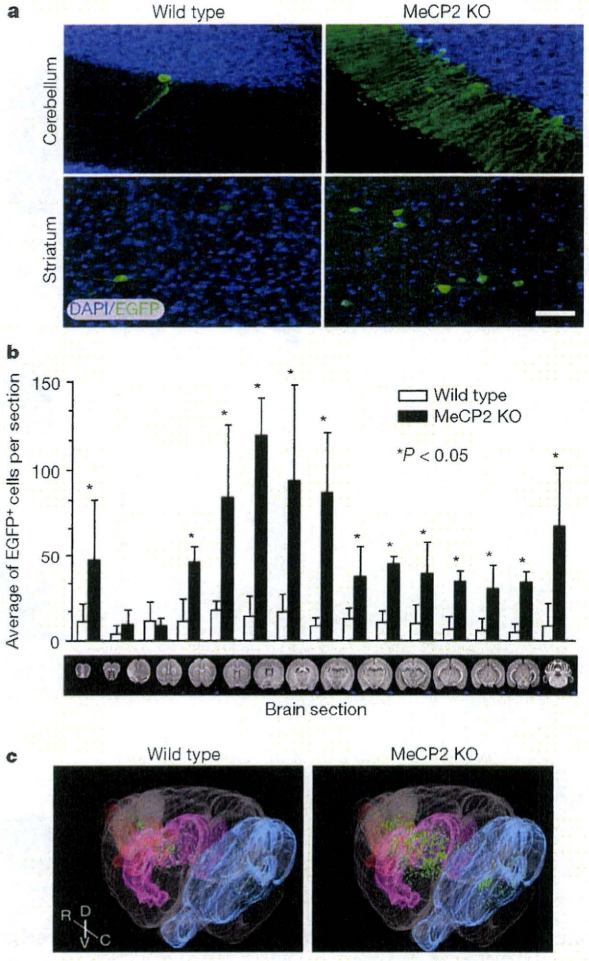

Figure 2 | MeCP2 modulates neuronal L1 retrotransposition *in vivo*. **a**, EGFP-positive cells, indicating *de novo* L1 retrotransposition, were found in several regions of the brain. The images were taken from sections that were highly affected by L1 retrotransposition. Bar, 30 μm. **b**, Quantification of brain sections in MeCP2 KO background revealed more EGFP-positive cells compared to wild type ($n = 6$ animals for each group). Error bars show s.d. **c**, Representative images from a three-dimensional reconstruction of wild-type and MeCP2 KO brains carrying the L1–EGFP transgene. Single dots (green) represent neurons that supported L1–EGFP retrotransposition. Olfactory bulb is shown in red, striatum in magenta and cerebellum in cyan. R, rostral; C, caudal; D, dorsal and V, ventral.

5S ribosomal RNA repetitive sequences (Fig. 3d). Another control experiment was performed using fibroblasts isolated from the two backgrounds (Fig. 3e). We did not observe a highly significant increase in L1 copy number in MeCP2 KO compared to wild type fibroblasts.

Mutations on the MeCP2 gene cause RTT, characterized by arrested development in early childhood and autistic behaviour at different levels of intensity[21]. To determine if L1 retrotransposition could occur in neuronal progenitor cells (NPC) derived from RTT patients, we generated induced pluripotent stem cells (iPSC) from a RTT patient's fibroblasts carrying a frameshift MeCP2 mutation and from a control, non-affected individual. All clones were pluripotent and able to produce NPC and neurons (Supplementary Fig. 5). Thus, we tested if the iPSC-derived NPC supported L1 retrotransposition.

NPC from both wild-type and RTT iPSC expressed the neural markers Sox1, Musashi1, Nestin and Sox2 at similar rates at the time of the experiment (Supplementary Fig. 6a, b). RTT and wild-type cells were electroporated with the $L1_{RE3}$–EGFP reporter construct[22,23] (Fig. 4a). EGFP expression was detected in both wild-type and RTT cells (Fig. 4b). The frequency of EGFP-positive cells was approximately

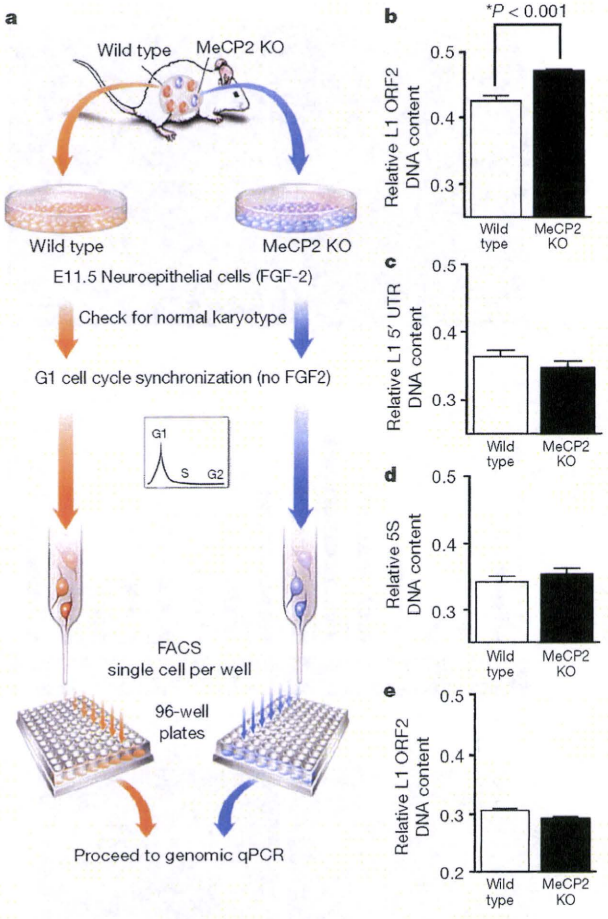

Figure 3 | Endogenous L1 retrotransposition in mouse neuroepithelial cells. **a**, Neuroepithelial cells harvested from embryonic day 11.5 (E11.5) sibling embryos were synchronized and sorted in individual wells followed by qPCR. **b**, Neuroepithelial cells in the MeCP2 KO background had higher L1 ORF2 DNA content than wild-type cells ($P < 0.001$). **c**, L1 5′UTR primers did not reveal a significant increase in copy number in MeCP2 KO background. **d**, Non-mobile 5S ribosomal genes were used as controls. **e**, The difference in the amount of L1 ORF2 DNA in fibroblasts from the different genetic backgrounds was smaller than in the neural lineage. All experiments show experimental triplicates ($n = 192$ cells for each primer pair). Error bars in all panels show s.e.m.

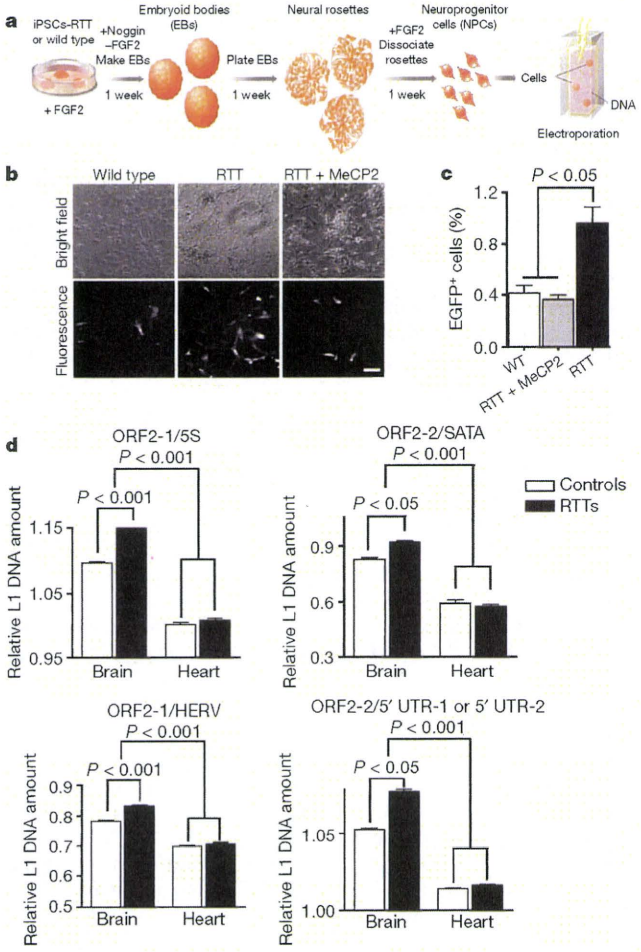

Figure 4 | L1 retrotransposition in RTT patients. **a**, Schematic view of the NPC differentiation from iPSC followed by $L1_{RP3}$–EGFP electroporation. **b**, Representative images of iPSC-derived NPC expressing EGFP after L1 retrotransposition. Bar, 30 μm. **c**, Quantification of the EGFP-positive cells after transfection. **d**, Primers for ORF2 were used to multiplex with primers for control sequences, such as the 5S ribosomal gene (5S), the satellite alpha (SATA) region, the human endogenous retrovirus H (HERV) sequence and the 5′UTR. The inverse ratio of ORF2/5S represents the amount of L1 ORF2 sequence in each sample ($n = 5$ individuals per group). Similar results were obtained when different primers/probe for ORF2 (ORF2-2) were multiplex/normalized to other control sequences, using two pair of primers (5′UTR-1 or 5′UTR-2). Error bars show s.e.m, and the experiments were performed in triplicate.

twofold higher in RTT than in control cells. Moreover, MeCP2 complementation reduced the levels of EGFP-positive cells in RTT NPC (Fig. 4b, c and Supplementary Fig. 6c). PCR confirmed the presence of the retrotransposed EGFP and sequencing confirmed the precise splicing of the intron (Supplementary Fig. 6d). We concluded that L1 activity could be facilitated by loss of MeCP2 function in human cells. We extended the iPSC findings *in vivo* using post mortem human tissues. To analyse the amounts of L1 retrotransposition in RTT patients and controls, brain and heart tissue was obtained from the same individuals. After genomic DNA extraction, a qPCR was used to compare the number of L1 ORF2 sequences normalized by four distinct non-mobile repetitive sequences. The number of L1 ORF2 sequences in the brains of RTT patients was significantly higher than in age/gender-matched controls (Fig. 4d). Moreover, the number of ORF2 sequences was higher in brain tissues in both controls and RTT patients when compared to heart tissue from the same individuals.

Our findings support previous data demonstrating that L1 5′UTR sequences are MeCP2 targets that may be subjected to methylation-dependent repression[15,17]. However, we cannot exclude an indirect effect of MeCP2 in regulating genes involved in L1 expression and/or in changing the chromatin epigenetic landscape to facilitate *de novo* L1 insertions. An additive effect of multiple mechanisms is likely. Using different strategies, we have shown that L1 retrotransposition can be modulated by MeCP2. First, we demonstrated that MeCP2 can downregulate L1 promoter activity. Second, L1 retrotransposition from the L1–EGFP transgenic mice was significantly higher in the brains of a MeCP2 KO background than in a wild-type sibling animal. The L1–EGFP indicator system underestimates the actual capacity of retrotransposition and does not take into account insertions that truncate or silence the reporter cassette, *in trans* retrotransposition of *Alu* sequences or other RNAs[24–26]. Third, we developed a new technique based on single-cell genomic qPCR to measure the relative abundance of L1 sequences, revealing that MeCP2 KO neuroepithelial cells have more L1 sequences in the genome than wild-type cells. Lastly, RTT-NPC showed a higher L1 retrotransposition frequency than control cells. A qPCR experiment extended these observations to human brain samples from RTT patients compared to controls.

Our data provide evidence of a role for DNA methylation-dependent MeCP2 activity in controlling L1 mobility in the nervous system. Re-activation of MeCP2 expression was shown to reverse some of the neurological symptoms in MeCP2 KO mice[27]. The high rates of neuronal retrotransposition in the MeCP2 KO mice and RTT patients may be a consequence, rather than a cause, of the disease process. Nonetheless, new somatic insertions, especially at early developmental stages, may contribute to the genetic and epigenetic status of mature neurons at later stages of life. Early developmental structural and functional modulations could have potential consequences for RTT, where the detrimental effects of MeCP2 mutation occur at later postnatal stages. It is plausible to conclude that the RTT process leads to an increased rate of somatic mutations in the brain. Increased L1 neuronal retrotransposition is a novel and unexpected characteristic of RTT pathology. Our findings add a new layer of complexity to the understanding of genomic plasticity and may have direct implications for individual variation and for neurological diseases.

METHODS SUMMARY

For the *luciferase* activity experiments, rat neural stem cells were isolated, characterized and cultured as described[28]. Neuroepithelial cells from time-pregnant midgestation (embryonic day 11.5) telencephalons from male wild-type, MBD1 KO, and MeCP2 KO sibling mouse embryos, from the same genetic background (C57BL/6J) were isolated. Cells were cultured for two to three passages in Dulbecco's modified Eagle's medium (DMEM) F12 media with N2 supplement and fibroblast growth factor 2 (FGF2) as described elsewhere[29]. Plasmid and siRNA transfections were performed by electroporation (Lonza/Amaxa Biosystem). Luciferase activity was measured with the Dual-Luciferase reporter assay system (Promega) according to the manufacturer's protocol. Chromatin immunoprecipitation (ChIP) assays were performed following the manufacturer's protocol using a kit from Millipore/Upstate. Antibodies used were anti-MeCP2 and IgG (Upstate). After immunoprecipitation, recovered chromatin fragments were subjected to PCR using primers for the rat L1 sequence. qPCR values were normalized to the IgG precipitation and shown as fold enrichment. For human iPSC derivation, RTT and control fibroblasts were infected with retroviral vectors containing the *Oct4*, *c-Myc*, *Klf4* and *Sox2* human cDNAs as described previously by Yamanaka's group[30]. iPSC-derived neural progenitors were electroporated (Lonza/Amaxa Biosystem) with L1–EGFP plasmid and FACS sorted for EGFP to quantify L1 *de novo* insertion. Single-cell genomic quantitative PCR (qPCR) was performed in cell-cycle-arrested neuroepithelial cells and fibroblasts from wild-type and MeCP2 KO mice. The plates containing one cell per well were then snap frozen at −80 °C until the day of the qPCR. The qPCR was performed using the protocol available on the manufacturer's website (Applied Biosystems). Briefly, a solution containing forward/reverse primers and SYBR Green PCR Master Mix was added to the previously sorted cells and the detection of DNA products was carried out in an ABI PRISM 7900HT Sequence Detection System. For multiplex genomic qPCR in human tissues the qPCR strategy and L1 copy estimation were done as previously described[8].

Received 27 April; accepted 30 September 2010.

Published online XX 2010.

1. Lander, E. S. *et al.* Initial sequencing and analysis of the human genome. *Nature* **409,** 860–921 (2001).
2. Gibbs, R. A. *et al.* Genome sequence of the Brown Norway rat yields insights into mammalian evolution. *Nature* **428,** 493–521 (2004).
3. Mouse Genome Sequencing Consortium. Initial sequencing and comparative analysis of the mouse genome. *Nature* **420,** 520–562 (2002).
4. Kazazian, H. H. Jr. Mobile elements and disease. *Curr. Opin. Genet. Dev.* **8,** 343–350 (1998).
5. Han, J. S., Szak, S. T. & Boeke, J. D. Transcriptional disruption by the L1 retrotransposon and implications for mammalian transcriptomes. *Nature* **429,** 268–274 (2004).
6. Perepelitsa-Belancio, V. & Deininger, P. RNA truncation by premature polyadenylation attenuates human mobile element activity. *Nature Genet.* **35,** 363–366 (2003).
7. Muotri, A. R. *et al.* Somatic mosaicism in neuronal precursor cells mediated by L1 retrotransposition. *Nature* **435,** 903–910 (2005).
8. Coufal, N. G. *et al.* L1 retrotransposition in human neural progenitor cells. *Nature* **460,** 1127–1131 (2009).
9. Muotri, A. R., Zhao, C., Marchetto, M. C. & Gage, F. H. Environmental influence on L1 retrotransposons in the adult hippocampus. *Hippocampus* **19,** 1002–1007 (2009).
10. Kuwabara, T. *et al.* Wnt-mediated activation of NeuroD1 and retro-elements during adult neurogenesis. *Nature Neurosci.* **12,** 1097–1105 (2009).
11. Muotri, A. R. & Gage, F. H. Generation of neuronal variability and complexity. *Nature* **441,** 1087–1093 (2006).
12. Singer, T., McConnell, M. J., Marchetto, M. C., Coufal, N. G. & Gage, F. H. LINE-1 retrotransposons: mediators of somatic variation in neuronal genomes? *Trends Neurosci.* **33,** 345–354 (2010).
13. Nan, X. *et al.* Transcriptional repression by the methyl-CpG-binding protein MeCP2 involves a histone deacetylase complex. *Nature* **393,** 386–389 (1998).
14. Jones, P. L. *et al.* Methylated DNA and MeCP2 recruit histone deacetylase to repress transcription. *Nature Genet.* **19,** 187–191 (1998).
15. Yu, F., Zingler, N., Schumann, G. & Stratling, W. H. Methyl-CpG-binding protein 2 represses LINE-1 expression and retrotransposition but not Alu transcription. *Nucleic Acids Res.* **29,** 4493–4501 (2001).
16. Zhao, X. *et al.* Mice lacking methyl-CpG binding protein 1 have deficits in adult neurogenesis and hippocampal function. *Proc. Natl Acad. Sci. USA* **100,** 6777–6782 (2003).
17. Klose, R. J. *et al.* DNA binding selectivity of MeCP2 due to a requirement for A/T sequences adjacent to methyl-CpG. *Mol. Cell* **19,** 667–678 (2005).
18. Rowe, H. M. *et al.* KAP1 controls endogenous retroviruses in embryonic stem cells. *Nature* **463,** 237–240 (2010).
19. Grimaldi, G., Skowronski, J. & Singer, M. F. Defining the beginning and end of *KpnI* family segments. *EMBO J.* **3,** 1753–1759 (1984).
20. Moran, J. V. & Gilbert, N. in *Mobile DNA II,* Vol. 2 (eds Craig, N. L., Craigie, R., Gellert, M. & Lambowitz, A. M.) Ch. 35, 836–869 (ASM Press, 2002).
21. Amir, R. E. *et al.* Rett syndrome is caused by mutations in X-linked *MECP2*, encoding methyl-CpG-binding protein 2. *Nature Genet.* **23,** 185–188 (1999).
22. Moran, J. V. *et al.* High frequency retrotransposition in cultured mammalian cells. *Cell* **87,** 917–927 (1996).
23. Ostertag, E. M., Prak, E. T., DeBerardinis, R. J., Moran, J. V. & Kazazian, H. H. Jr. Determination of L1 retrotransposition kinetics in cultured cells. *Nucleic Acids Res.* **28,** 1418–1423 (2000).
24. Esnault, C., Maestre, J. & Heidmann, T. Human LINE retrotransposons generate processed pseudogenes. *Nature Genet.* **24,** 363–367 (2000).
25. Dewannieux, M., Esnault, C. & Heidmann, T. LINE-mediated retrotransposition of marked Alu sequences. *Nature Genet.* **35,** 41–48 (2003).
26. Wei, W. *et al.* Human L1 retrotransposition: *cis* preference versus *trans* complementation. *Mol. Cell. Biol.* **21,** 1429–1439 (2001).
27. Guy, J., Gan, J., Selfridge, J., Cobb, S. & Bird, A. Reversal of neurological defects in a mouse model of Rett syndrome. *Science* **315,** 1143–1147 (2007).
28. Palmer, T. D., Takahashi, J. & Gage, F. H. The adult rat hippocampus contains primordial neural stem cells. *Mol. Cell. Neurosci.* **8,** 389–404 (1997).
29. Nakashima, K. *et al.* Synergistic signaling in fetal brain by STAT3-Smad1 complex bridged by p300. *Science* **284,** 479–482 (1999).
30. Takahashi, K. *et al.* Induction of pluripotent stem cells from adult human fibroblasts by defined factors. *Cell* **131,** 861–872 (2007).

Supplementary Information is linked to the online version of the paper at www.nature.com/nature.

Acknowledgements A.R.M. is supported by the National Institutes of Health through the NIH Director's New Innovator Award Program, 1-DP2-OD006495-01 and by the Emerald Foundation. F.H.G. is supported by the Mathers Foundation, Lookout Fund, and NIH/NINDS R01MH088485. The authors would like to thank A. Huynh, B. Aimone, K. Stecker, B. Berg and D. Sepp for help during the 3D brain model assembly, J. Moran and J. Garcia-Perez for discussion and critical review of the manuscript, M. Gage for editorial comments, and B. Moddy and G. Peng for experimental assistance.

Author Contributions A.R.M. and M.C.N.M. are the leading authors. They contributed to the concept, designed and performed the experiments, analysed the data, and wrote the manuscript. N.G.C. performed and analysed qPCR experiments. R.O. performed tissue culture experiments and quantification. G.Y. helped with statistical analysis and data interpretation. K.N. contributed reagents, and performed data analyses and manuscript revision. F.H.G. contributed to the concept, analysed the data and revised the manuscript.

Author Information Reprints and permissions information is available at www.nature.com/reprints. The authors declare no competing financial interests. Readers are welcome to comment on the online version of this article at www.nature.com/nature. Correspondence and requests for materials should be addressed to A.R.M. (muotri@ucsd.edu) or F.H.G. (gage@salk.edu).

Neurons derived from transplanted neural stem cells restore disrupted neuronal circuitry in a mouse model of spinal cord injury

Masahiko Abematsu,[1,2] Keita Tsujimura,[1] Mariko Yamano,[3] Michiko Saito,[4] Kenji Kohno,[4] Jun Kohyama,[1] Masakazu Namihira,[1] Setsuro Komiya,[2] and Kinichi Nakashima[1]

[1]Laboratory of Molecular Neuroscience, Graduate School of Biological Sciences, Nara Institute of Science and Technology, Ikoma, Japan. [2]Department of Orthopaedic Surgery, Graduate School of Medical and Dental Sciences, Kagoshima University, Kagoshima, Japan. [3]Department of Comprehensive Rehabilitation, Osaka Prefecture University, Habikino, Japan. [4]Laboratory of Molecular and Cell Genetics, Graduate School of Biological Sciences, Nara Institute of Science and Technology, Ikoma, Japan.

The body's capacity to restore damaged neural networks in the injured CNS is severely limited. Although various treatment regimens can partially alleviate spinal cord injury (SCI), the mechanisms responsible for symptomatic improvement remain elusive. Here, using a mouse model of SCI, we have shown that transplantation of neural stem cells (NSCs) together with administration of valproic acid (VPA), a known antiepileptic and histone deacetylase inhibitor, dramatically enhanced the restoration of hind limb function. VPA treatment promoted the differentiation of transplanted NSCs into neurons rather than glial cells. Transsynaptic anterograde corticospinal tract tracing revealed that transplant-derived neurons reconstructed broken neuronal circuits, and electron microscopic analysis revealed that the transplant-derived neurons both received and sent synaptic connections to endogenous neurons. Ablation of the transplanted cells abolished the recovery of hind limb motor function, confirming that NSC transplantation directly contributed to restored motor function. These findings raise the possibility that epigenetic status in transplanted NSCs can be manipulated to provide effective treatment for SCI.

Introduction

Numerous studies (1–18) have indicated that a variety of treatments, such as administration of antibodies against myelin-associated neurite growth inhibitors (4, 5, 16) and neurotrophic factors (12, 13), can yield limited restorative benefits for spinal cord injury (SCI), but the mechanistic basis of symptomatic improvement is far from clear. Because of their ability to self renew, to differentiate into multiple lineages, and to migrate toward damaged sites, neural stem cells (NSCs) are currently considered to be promising components of cell-replacement strategies aimed at treating CNS injuries (7–11, 14, 15).

Two desirable objectives of cell-based therapeutics are to induce trophic reactions, such as the production of extracellular matrix and diffusible factors, and to replace cells lost through injury or disease with transplant-derived cells, such as new oligodendrocytes and neurons, that will enhance the regenerative responses of the host CNS. Trophic factors secreted from transplanted cells have been shown to support neuronal survival and neurite outgrowth (12, 13), while other studies report that transplanted oligodendrocyte precursor cells enhance remyelination of remaining neuronal axons, leading to restoration of locomotion after SCI (9, 15). Stem cell–derived neuronal supplementation in the injured spinal cord also induces partial recovery, although a direct contribution of such neurons to the reconstruction of disrupted neuronal circuits has not been demonstrated (7, 10, 11).

In the severest CNS injuries, many neurons sustain direct damage and disrupted neuronal circuits have to be restored. Inflammatory cytokines are upregulated at lesion sites in the CNS (19–21), but their effect is to promote astrocytic differentiation. Moreover, while exogenous NSCs that are transplanted into the injured CNS undergo proliferation, the vast majority of newly generated cells differentiate into astrocytes (7, 21, 22). This strong bias toward astrocytic differentiation at the expense of neuronal differentiation is one of the major current obstacles in regeneration therapy.

Valproic acid (VPA; 2-propylpentanoic acid) is an established drug in the long-term treatment of epilepsy (23). Recent experiments have further revealed that VPA can directly inhibit histone deacetylase (HDAC) activity and cause hyperacetylation of histones in 293T, Neuro2A, and teratocarcinoma F9 cells (24, 25), and we have also found that VPA induces neuronal differentiation but suppresses astrocytic and oligodendrocytic differentiation of NSCs (26). Taking advantage of these newly discovered effects of VPA, we report here that functional recovery in SCI model mice is dramatically improved by a combined treatment involving NSC transplantation and VPA administration. Furthermore, we reveal the precise mechanisms used to reconstruct the damaged corticospinal tract (CST); these differ from neurite regrowth and remyelination of host neurons, hitherto considered as the major reasons for functional recovery of SCI following NSC transplantation.

Results

Combined NSC transplantation and VPA administration improves functional recovery of hind limbs without CST axon reextension. As VPA has been shown to have effects that are likely to be beneficial to treatment of the injured CNS, such as neuroprotection (27–31), induction of neuronal differentiation (26), and promotion of neurite outgrowth (32), we examined the response of SCI model

Conflict of interest: The authors have declared that no conflict of interest exists.
Citation for this article: *J Clin Invest.* 2010;120(9):3255–3266. doi:10.1172/JCI42957.

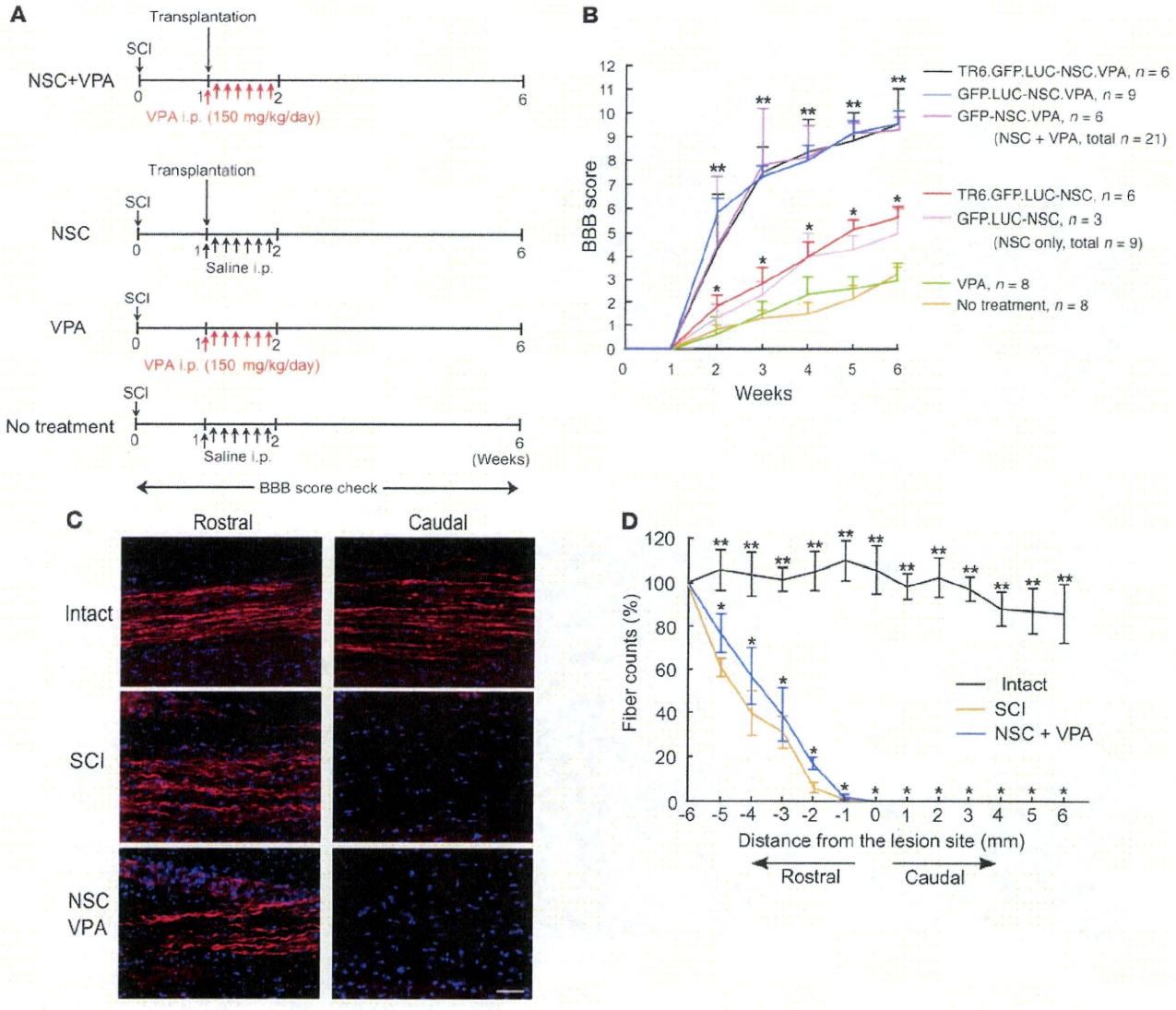

Figure 1

A combination of NSC transplantation and VPA administration improves functional recovery of hind limbs without CST axon reextension. (**A**) Schematic of the NSC transplantation and VPA injection protocol. (**B**) Time course of functional recovery of hind limbs after SCI. GFP-NSCs, GFP.LUC-NSCs, and TR6.GFP.LUC-NSCs were transplanted into the SCI epicenter 7 days after injury as indicated. Combined treatment with NSC transplantation and VPA administration resulted in the greatest functional recovery. Data represent mean ± SEM. $^{**}P < 0.001$ compared with SCI models with no treatment; $^{*}P < 0.01$ compared with SCI models with no treatment (repeated measures ANOVA). NSC+VPA, total $n = 21$. (**C**) Representative pictures of BDA-labeled CST fibers at 5 mm rostral and 5 mm caudal to the lesion site. BDA was injected into the motor cortices 12 weeks after SCI. 2 weeks after the injection, mice were fixed and spinal cord sections were stained. Representative results for a GFP-NSC–transplanted spinal cord are shown. Blue, Hoechst nuclear staining. Scale bar: 20 μm. (**D**) Quantification of the labeled CST fibers in the spinal cords of intact mice, SCI mice receiving no treatment, and SCI mice undergoing combined NSC/VPA treatment. Eight 30-μm–thick serial parasagittal sections from individual spinal cords were evaluated. The *x* axis indicates specific locations along the rostrocaudal axis of the spinal cord, and the *y* axis indicates the ratio of the number of BDA-labeled fibers at the indicated site to that at 6 mm rostral to the lesion site (Th9). $^{**}P < 0.001$ compared with SCI models without treatment; $^{*}P = 0.188$ There is no significant difference in the number of BDA-labeled fibers between NSC+VPA-treated mice (blue line) and SCI model mice with no treatment (yellow line) (repeated measures ANOVA). All data shown are from at least 3 experiments in parallel conditions, with error bars representing SEM.

mice to different combinations of VPA administration and NSC transplantation. We prepared NSCs from embryonic forebrains of 3 different Tg mouse lines ubiquitously expressing either GFP (GFP-Tg) (33), GFP and LUC (GFP.LUC-Tg), or GFP, LUC, and the diphtheria toxin (DT) receptor human heparin-binding EGF-like growth factor (TR6) (TR6.GFP.LUC-Tg) (see Methods). The expression of GFP, LUC, and TR6 in NSCs enabled us to distinguish transplanted cells from host cells, to trace the survival of transplanted cells based on LUC activity in a noninvasive fashion, and to specifically ablate transplanted cells (see below), respectively. To obtain a homogeneous population of NSCs, we used adherent monolayer culture (34–36). The embryonic forebrains were

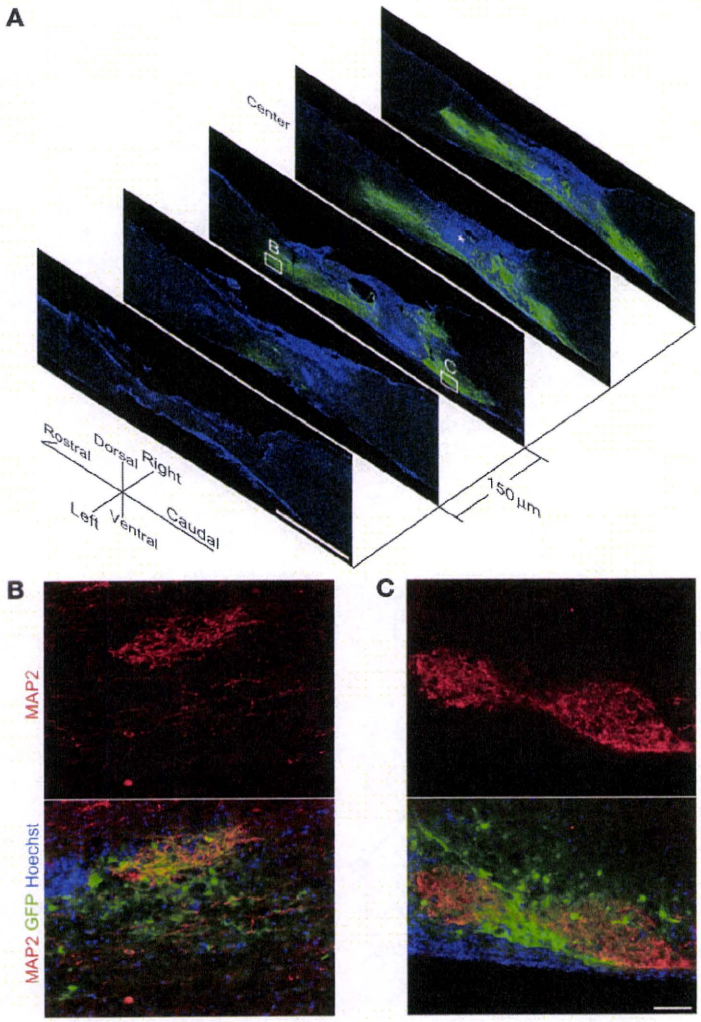

Figure 2

Transplanted NSCs migrate from the injection site and encompass the lesion site. Representative results of GFP-NSC–transplanted SCI model mice are shown. (**A**) A series of immunostaining images of injured spinal cord at 6 weeks after injury. SCI mice received combination treatment with NSC transplantation and VPA administration. Specimens were picked up every 150 μm and stained with anti-GFP (green) and MAP2 (not shown) antibodies and Hoechst (blue). The epicenter of the SCI is indicated (*). Scale bar: 1 mm. (**B** and **C**) Higher-magnification images of the white boxes in **A**. GFP-positive transplanted NSCs differentiated into MAP2-positive neurons and extended their processes. Scale bar: 50 μm.

dissociated and cultured with EGF and basic FGF (bFGF) (36) (Supplemental Figure 1, A and B; supplemental material available online with this article; doi:10.1172/JCI42957DS1). These cells uniformly expressed the stem cell markers Sox2 and nestin but did not express differentiation markers (Supplemental Figure 1, C and D). Under the appropriate conditions for each lineage, these NSCs differentiated into neurons, astrocytes, or oligodendrocytes (Supplemental Figure 1, E and F). NSCs from different Tg mice behaved similarly in these culture conditions (data not shown). NSCs that had been cultured and passaged 5–10 times in the presence of both EGF and bFGF to maintain the undifferentiated state were used for transplantation studies.

Undifferentiated NSCs were transplanted into the SCI epicenter 7 days after injury. Nontransplanted control and transplanted mice were then intraperitoneally administered VPA or saline daily for 7 days (Figure 1A), whereafter we monitored their hind limb motor function using the open field locomotor scale (BBB score) (7–9, 37) for 6 weeks. Remarkably, we found that the simultaneous treatment of SCI model mice with NSCs and VPA resulted in a dramatic recovery of hind limb function compared with either treatment alone (Figure 1B and Supplemental Videos 1–4). There were no significant differences among the data obtained from each SCI model mouse group transplanted with the 3 distinct NSCs. Functional recovery of each treated SCI model mouse reached a plateau at around 6 weeks, the level of which was sustained for more than 3 months. Since mice treated with VPA alone showed no further improvement compared with untreated mice, it is most likely that VPA affected the function of transplanted cells.

We next sought to determine the basis for this improvement in locomotor function. Since transplanted NSCs have been reported to play a supportive role in the reextension of injured axons (14), we analyzed whether CST axons were regenerated by anterograde labeling using biotinylated dextran amine (BDA) (6, 16, 17). Because BDA was injected into the motor cortex, only the axons of first-order neurons in the CST could be visualized (Figure 1C). In our SCI model mice, the caudal part of the injured site was completely devoid of CST axons (Figure 1, C and D), and the same was true in mice that had undergone combined NSC transplantation and VPA administration (Figure 1, C and D). These data indicated that CST axons did not reextend in mice treated with both NSCs and VPA and therefore that some other mechanism was responsible for the animals' dramatic functional locomotor improvement.

Transplanted NSCs encompass the lesion site and extend their processes. Given that host CST axon reextension was not involved in the observed hind limb recovery, we decided to focus on the transplanted cells. We analyzed the migration, morphology, neuronal marker expression, and viability of these cells after coadministration with VPA. Transplant-derived cells migrated to both rostral and caudal areas and displayed processes that extended into the gray matter and dorsal funiculus within 5 weeks of transplantation (Figure 2). Between 20% and 40% of the transplanted cells were found to be surviving in the injured spinal cord after 8 weeks, and 17% still remained viable more than 1 year after transplantation (data not shown). About 20% of the surviving cells had differentiated into microtubule-associated protein 2–positive (MAP2-positive) neurons with elongated processes within 5 weeks after transplantation (Figure 2, B and C, and Figure 3, E and F). Survival of the transplanted NSCs was not significantly influenced by VPA administration (Supplemental Figure 8).

HDAC inhibition promotes neuronal differentiation of NSCs and is critical for transplantation-induced hind limb recovery. In contrast to previous studies, which have indicated that very few transplanted NSCs differentiate into neurons in the injured CNS environment (8, 10, 11, 20), many neurons were observed in the spinal cord after coadministration with VPA. We next examined in more detail the contribution of VPA to differentiation of cultured and transplanted NSCs. To analyze differentiation in vitro, NSCs were treated with either

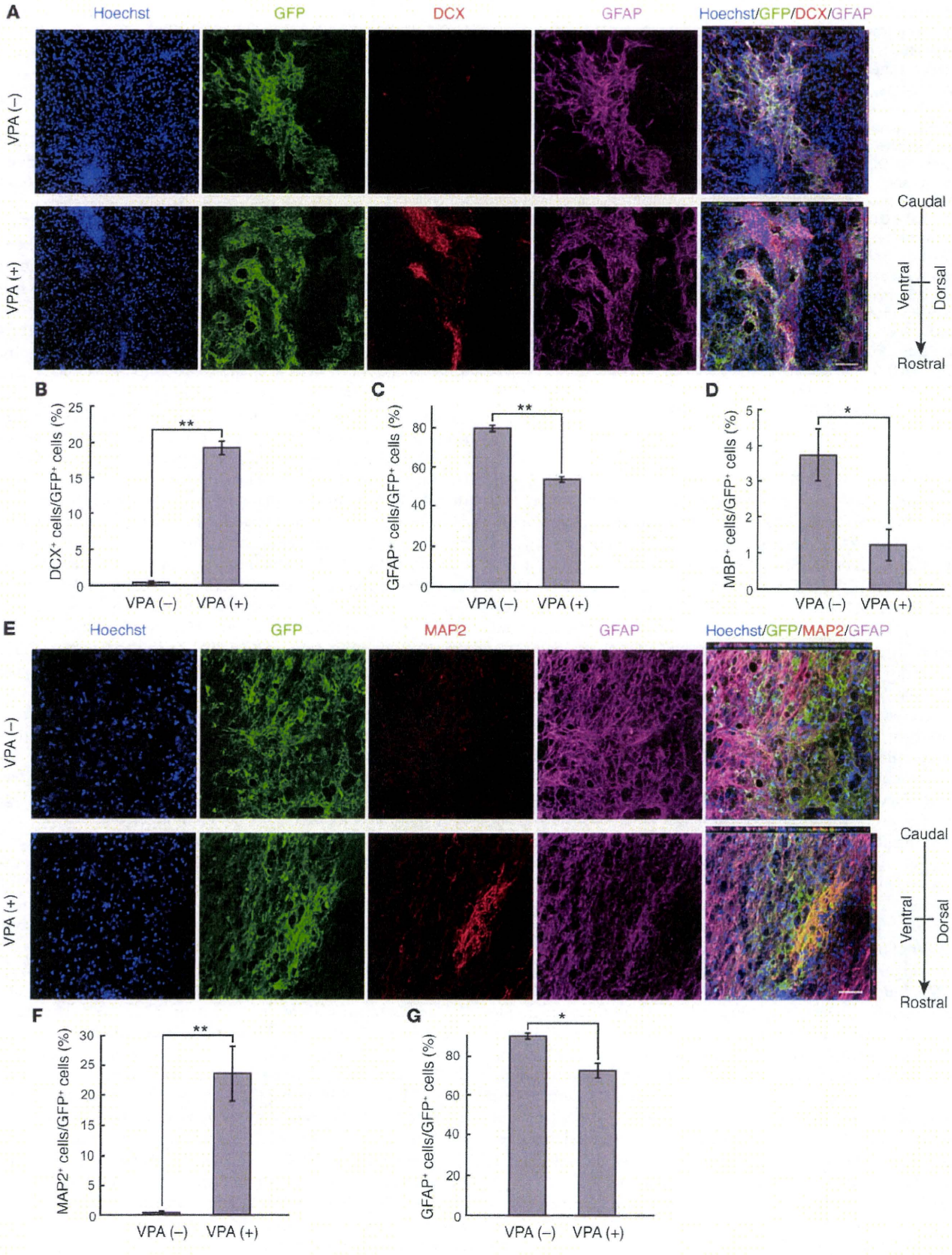
A
Hoechst
GFP
DCX
GFAP
Hoechst/GFP/DCX/GFAP
VPA (–)
VPA (+)
Caudal
Ventral
Dorsal
Rostral
B
DCX+ cells/GFP+ cells (%)
25
20
15
10
5
0
**
VPA (–)
VPA (+)
C
GFAP+ cells/GFP+ cells (%)
80
60
40
20
0
**
VPA (–)
VPA (+)
D
MBP+ cells/GFP+ cells (%)
5
4
3
2
1
0
*
VPA (–)
VPA (+)
E
Hoechst
GFP
MAP2
GFAP
Hoechst/GFP/MAP2/GFAP
VPA (–)
VPA (+)
Caudal
Ventral
Dorsal
Rostral
F
MAP2+ cells/GFP+ cells (%)
30
25
20
15
10
5
0
**
VPA (–)
VPA (+)
G
GFAP+ cells/GFP+ cells (%)
80
60
40
20
0
*
VPA (–)
VPA (+)

Figure 3
VPA promotes neuronal differentiation of transplanted NSCs. Representative results of GFP-NSC–transplanted SCI model mice are shown. (**A**) Confocal images of NSCs 1 week after transplantation into the injured spinal cords. Spinal cord sections from VPA-treated (+) and untreated (–) mice were stained with anti-GFP (green), anti-doublecortin (DCX) (immature neuronal marker, red) and anti-GFAP (magenta) antibodies, and Hoechst (blue). VPA administration resulted in an increase in the number of DCX-positive neuronal precursors among transplanted cells (lower panel). Scale bar: 20 μm. (**B–D**) The percentages of DCX-, GFAP-, and MBP-positive cells in GFP-positive transplanted cells were quantified. $^{**}P < 0.01$; $^{*}P < 0.05$ compared with controls (Student's *t* test). (**E**) Confocal images of NSCs 5 weeks after transplantation into injured spinal cords. Spinal cord sections from VPA-treated (+) and untreated (–) mice were stained with anti-GFP (green), anti-MAP2 (neuronal marker, red) and anti-GFAP (magenta) antibodies, and Hoechst (blue). VPA administration increased the numbers of MAP2-positive neurons (lower panel). Scale bar: 20 μm. (**F** and **G**) The percentages of cells positive for MAP2 or GFAP in GFP-positive transplanted cells in **E** were quantified. $^{**}P < 0.01$; $^{*}P < 0.05$ compared with control (Student's *t* test). All data shown in **B–D**, **F**, and **G** are from at least 15 confocal images of 3 individuals in parallel experiments, with error bars representing the SD.

VPA or valpromide (VPM), an amide analog of VPA that is also an antiepileptic but is not an HDAC inhibitor (24), under differentiation culture conditions. VPA enhanced histone acetylation (Supplemental Figure 2A) and promoted neuronal differentiation and neurite outgrowth of the NSCs (Supplemental Figure 3, A–C); it also inhibited astrocytic and oligodendrocytic differentiation of NSCs (Supplemental Figure 3, D–G). A different HDAC inhibitor, trichostatin A (TSA), also enhanced histone acetylation (Supplemental Figure 2A) and neuronal differentiation of NSCs (not shown) (26). In contrast, VPM neither enhanced histone acetylation nor induced neuronal differentiation, suggesting that HDAC inhibition has an important role in regulating fate determination in NSCs.

We then assessed the histone acetylation status and differentiation profiles of transplanted NSCs. VPA administration enhanced histone acetylation in transplanted cells in the spinal cord (Supplemental Figure 2, B and C). When we examined the differentiation status of transplanted cells 1 week after transplantation, neuronal but not glial differentiation was greatly enhanced by VPA administration (Figure 3, A–D, and Supplemental Figure 4A). A similar differentiation tendency of transplanted NSCs to that at 1 week was observed at 5 weeks after transplantation: there was a dramatic increase in the number of cells positive for MAP2 (a relatively late differentiation marker of neurons in comparison with DCX) in VPA-administered mice (Figure 3, E–G, and Supplemental Figure 4B). Furthermore, VPM administration to the SCI mice neither promoted neuronal differentiation nor enhanced hind limb motor function, suggesting that HDAC inhibition has an essential role in regulating fate determination of transplanted NSCs and improvement of motor function in vivo (Supplemental Figure 5, A–C). In light of the above findings that the percentage of neurons generated from transplanted NSCs increased dramatically with VPA administration, whereas those of astrocytes and oligodendrocytes declined, we anticipated that these neurons would be likely to play a major role in regenerating the disrupted neuronal circuitry of the injured spinal cord.

Transplant-derived neurons reconstruct disrupted neuronal circuits in a relay manner. We next asked how the disrupted neuronal circuits were regenerated following the combined treatment with NSC transplantation and VPA administration. Wheat germ agglutinin (WGA), which can be transsynaptically transported, is one of the best known tracers of neural pathways (38). WGA protein can be transferred across synapses to second- and third-order neurons, permitting functional neuronal circuits to be tracked in the CNS. We injected WGA-expressing adenoviruses into the motor cortex of mouse brain 12 weeks after SCI. In uninjured mice, WGA was detected as intracellular granule-like structures in neurons localized in the ventral horn throughout the spinal cord (Figure 4, A and B). In untreated SCI model mice, WGA granules were almost completely absent from the caudal region below the injured site (Figure 4, A and C). Surprisingly, although we could not observe CST axonal reextension through the lesion site (Figure 1, C and D), WGA granules were clearly present in caudal large neurons located in the spinal cords of mice treated with both NSC and VPA (Figure 4, A and D). Intriguingly, moreover, transplant-derived neurons in or close to the lesion site contained WGA granules (Figure 4E), which were received from more rostral neurons. These data imply that WGA was conveyed through the lesion site to the caudal area via transplant-derived neurons. Considering this finding, together with the fact that WGA could be detected in caudal neurons without CST axonal reextension in mice that had undergone the combined treatment, it seemed conceivable that the transplant-derived neurons reconstructed the disrupted neuronal circuits, thereby acting as "relays" for transmitting signals between endogenous neurons whose interconnection had been abolished by the injury. In mice that received NSC transplantation alone after SCI, the percentage of WGA-positive cells among MAP2ab-positive cells in the caudal region was higher than that in untreated mice (Figure 4C) but lower than that in mice receiving combined NSC transplantation and VPA administration (Supplemental Figure 6), reflecting the degree of hind limb functional improvement (Figure 1C).

In support of the notion of a "relay" function for transplant-derived neurons, immunoelectron microscopy revealed that GFP-positive transplant-derived neurons received projections from endogenous neurons (Figure 5, A and B) and that the axon terminals of transplant-derived neurons made synapses with endogenous neurons localized in the ventral horn (Figure 5, C–E).

Transplanted cells contribute directly to functional recovery of hind limb movement in SCI mice. To determine whether the transplanted cells made a direct contribution to the functional recovery of hind limbs after SCI, we performed specific ablation of transplanted cells using the toxin receptor–mediated cell knockout (TRECK) method (Figure 6A and refs. 39, 40). For this purpose, we prepared NSCs from the embryonic forebrains of GFP.LUC Tg and TR6.GFP.LUC Tg mice (Figure 6A and Supplemental Figure 7, A and B). Almost all of the transplanted TR6.GFP.LUC-NSCs were specifically ablated following DT administration (Figure 6, B and C). Furthermore, after ablation of the transplanted cells, the BBB scores of SCI model mice that had undergone combined TR6.GFP.LUC-NSC transplantation and VPA administration declined rapidly to levels similar to those observed in untreated and VPA only–treated mice. These results were superimposed on the graph in Figure 1B, with the observation period extended to 12 weeks after SCI, as shown in Figure 6D (for clarity, the data for GFP-NSC.VPA and GFP.LUC-NS in Figure 1B were removed). These data indicate that the transplanted cells, in the presence of VPA, made a direct and major contribution to the functional recovery of hind limb movement in SCI model mice.

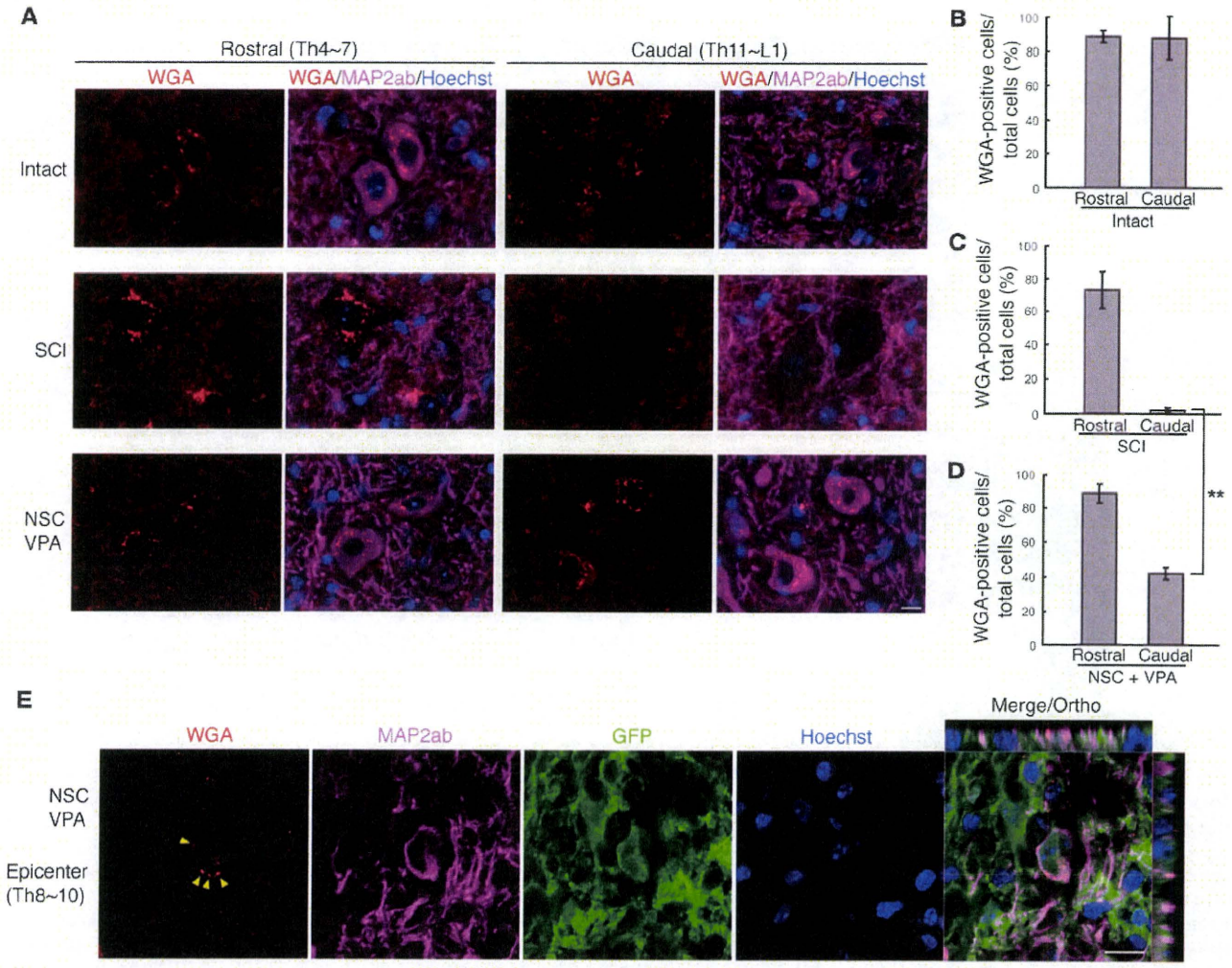

Figure 4

Transplant-derived neurons reconstruct disrupted neuronal circuits in a relay manner. (**A**) Representative pictures of WGA-labeled neuronal cell bodies located in the ventral horn at 14 weeks after SCI. Spinal cord sections were stained with anti-WGA (red) and -MAP2ab (magenta) antibodies and Hoechst (blue). Scale bar: 20 μm. Intense WGA immunoreactivity was observed as intracellular granule-like structures. Left panels show the rostral area (Th4–Th7), and right panels show the caudal area (Th11 to lumbar vertebra [L] 1). In uninjured mice, WGA injected into the bilateral motor cortices was transsynaptically transported to neurons in areas rostral and caudal to the injured site (top panels). In the SCI model mice that did not receive treatment, very little WGA was observed in caudal areas (middle panels). However, in spinal cords of animals that underwent dual treatment with NSC and VPA, WGA was clearly observed in neurons in the caudal areas (bottom panels). Representative results of GFP-NSC–transplanted SCI model mice are shown. (**B–D**) The percentages of WGA-positive cells in the neurons localized in the ventral horn were quantified. $^{**}P < 0.05$ (Student's *t* test). All data shown are from at least 30 images, containing more than 600 cells, from 3 individuals (5 images per area) in parallel experiments, with error bars representing SD. (**E**) Representative confocal images of WGA-labeled transplant-derived MAP2-positive neurons. Sections were stained with anti-WGA (red), anti-MAP2ab (magenta) and anti-GFP (green) antibodies, and Hoechst (blue). Granule-like WGA structures (yellow arrowheads) could be seen in the GFP and MAP2ab–double-positive transplant-derived neurons. Scale bar: 10 μm.

Both endogenous and transplant-derived local neurons play an important role in improving hind limb motor function. It has been shown recently that local neurons in the spinal cord play an important role in spontaneous functional recovery after SCI (41, 42). In our SCI model, we also observed slight but significant spontaneous recovery of hind limb function in untreated mice, and similar levels of recovery were sustained after ablation of transplanted cells (Figure 6D). We thus hypothesized that these recoveries were attributable to endogenous local neurons in the spinal cord. Furthermore, it seemed likely that the much higher recovery observed in mice with the combined treatment but without cell ablation (Figure 6D) was effected by transplant-derived local neurons in addition to the endogenous ones. To evaluate the involvement of these local neurons in our treatment regime, we divided each treated mouse group analyzed in Figure 6D into 2 subgroups (except for the "TR6.GFP.LUC-NCS–transplanted only" and "VPA-administered only" groups). The axon-sparing excitotoxin NMDA was injected at 12 weeks after SCI into the injury epicenter in the injured spinal cords of the mice in 1 subgroup for each treatment to ablate local neurons in the gray matter (43–45). In uninjured mice, NMDA injections had no significant effect on

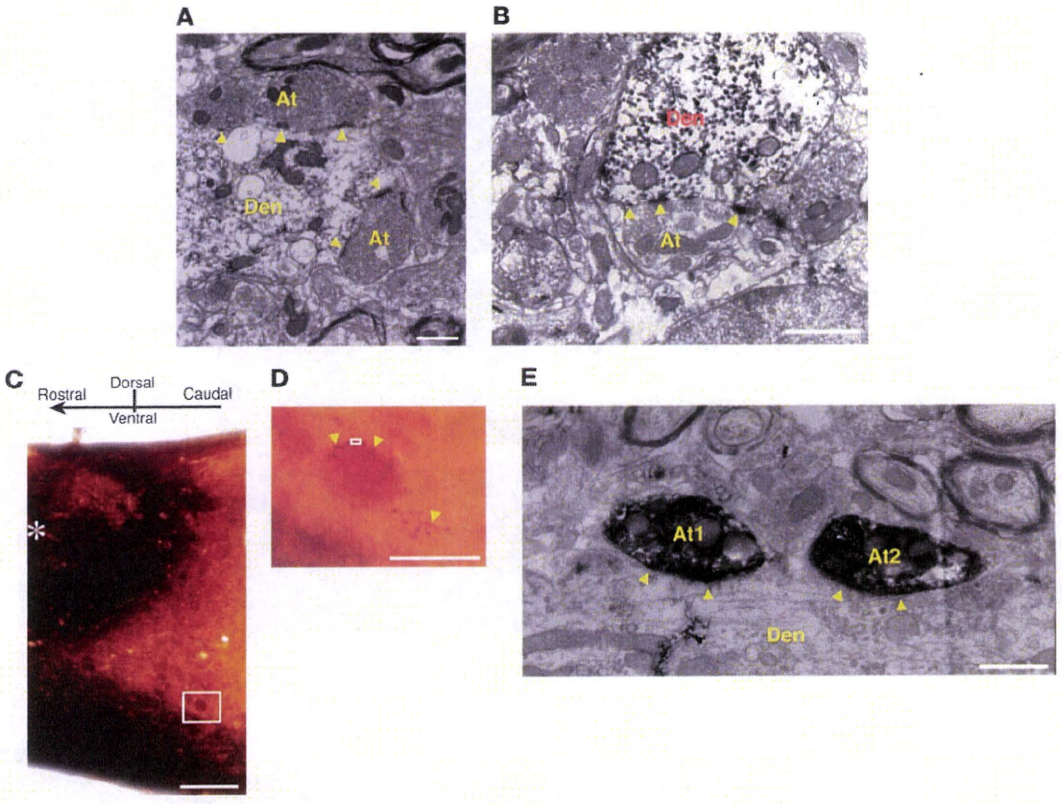

Figure 5
Transplant-derived neurons make synapses with endogenous neurons. (**A**) Immunoelectron microscopy image of a sagittal section of dual-treated (GFP-NSC and VPA) injured spinal cord (rostral area). A GFP-positive dendrite (Den) made synapses with GFP-negative endogenous axon termini (At) (yellow arrowheads). Scale bar: 1 μm. (**B**) In other rostral regions, a dendrite of a GFP-positive transplant-derived neuron made a synapse (yellow arrowheads) with the axon terminus of a GFP-negative endogenous neuron. Scale bar: 1 μm. (**C**) Sagittal section of dual-treated (NSC and VPA) injured spinal cord (caudal area) stained with anti-GFP antibody (dark brown). The epicenter of the SCI is indicated (*). Scale bar: 500 μm. (**D**) High-magnification image of a large neuron localized in the ventral horn in the white rectangle in **C**. GFP-positive transplanted neurons extended their processes toward an endogenous neuron (yellow arrowheads). Scale bar: 100 μm. (**E**) Immunoelectron microscopy image of the boxed area in **D**. GFP-positive axon termini made synapses with the dendrite of a GFP-negative endogenous large neuron (yellow arrowheads). Scale bar: 1 μm.

hind limb function (data not shown). However, as shown in Figure 6E, NMDA injections completely reversed both spontaneous and treatment-provoked functional recovery of hind limb movement in SCI model mice, indicating that both endogenous and transplant-derived local neurons indeed play an important role in the restoration of hind limb motor function.

Discussion

Over the last 3 decades, numerous strategies to cure CNS injuries, including SCI, have been devised and tested (1–18). Regeneration of injured neuronal circuits in the adult CNS is a multistep process: axons must extend their processes to contact appropriate neuronal targets and must then be remyelinated, and functional synapses need to form on the surfaces of the targeted neurons. Stem cell–derived cell supplementation to the injured spinal cord was previously shown to induce partial recovery (8, 9, 11, 15). However, the SCI models used in these studies involved moderate injury, so that hind limb motor function recovered spontaneously and sufficiently, even in untreated subjects, for the animals to be able to support their own weight and walk (BBB scores were approximately 10 to 13) within 3 weeks. In these studies, axons demyelinated by the injury were reportedly remyelinated by transplant-derived oligodendrocytes, leading to significant but minor improvements in BBB score (to approximately 12 to 16) over those observed in untreated mice.

In clinical practice, as treatment of moderate SCI has improved greatly with advanced surgical reconstruction techniques and better general management, the development of regenerative therapies for severer, recalcitrant forms of SCI is more pressing (46). Accordingly, we applied in this study a severe SCI model in which CST axons were completely disrupted (Figure 1C) to assess the effectiveness of our strategy. Hind limb motor function in untreated mice recovered only marginally (to a BBB score of ~4), whereas recovery improved dramatically, to the level at which mice could support their weight, as a consequence of the combined treatment with NSCs and VPA (BBB score ~9 to 10). Such a degree of improvement in hind limb function in severely injured mice has, to the best of our knowledge, never before been attained. Although a neuroprotective effect has been reported for VPA (27–31), this does not seem to be pertinent to the functional recovery of SCI because mice treated with VPA alone showed no

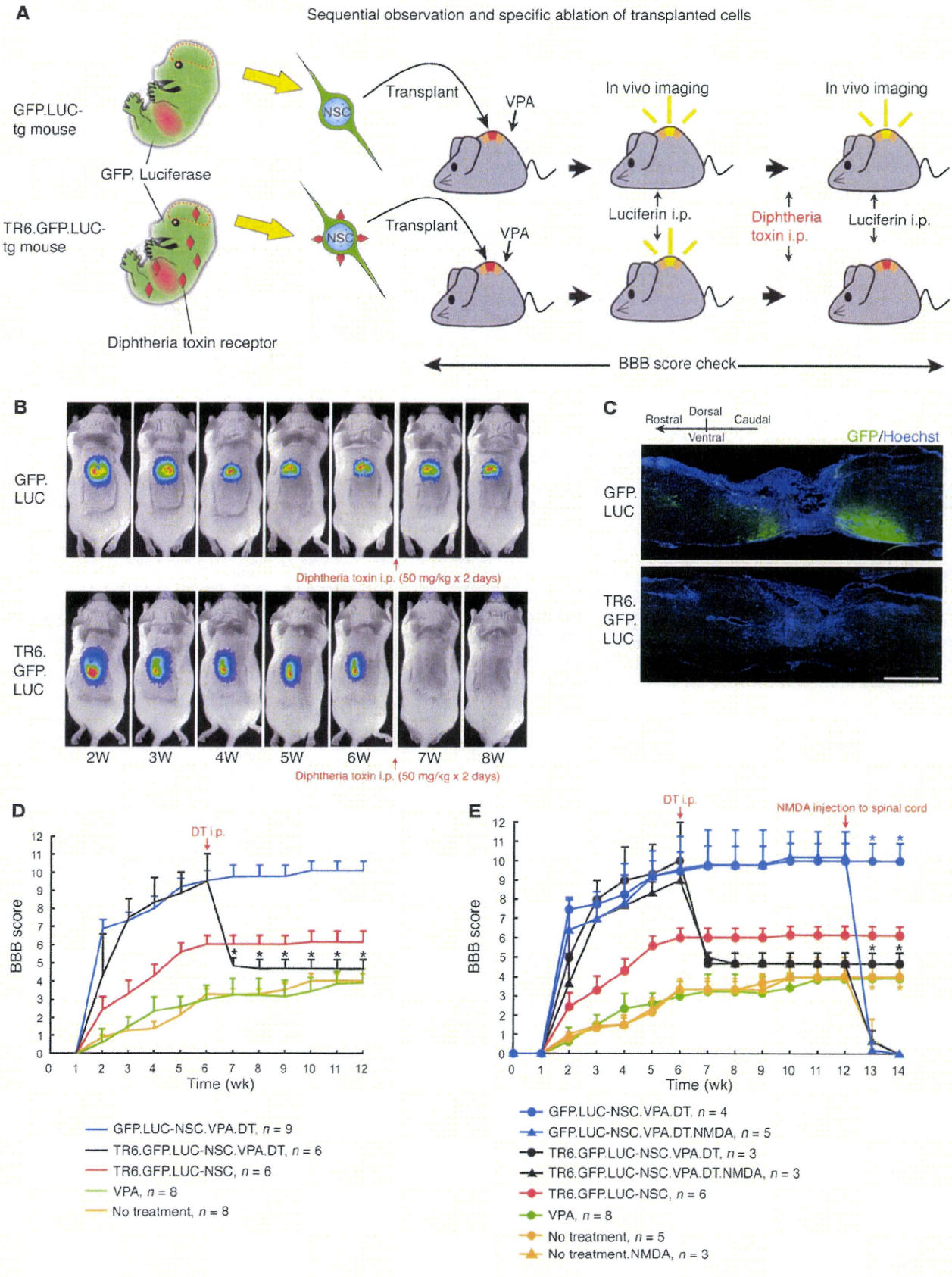
A
Sequential observation and specific ablation of transplanted cells
GFP.LUC-tg mouse
GFP, Luciferase
TR6.GFP.LUC-tg mouse
Diphtheria toxin receptor
NSC
Transplant
VPA
In vivo imaging
Luciferin i.p.
Diphtheria toxin i.p.
BBB score check
B
GFP.LUC
TR6.GFP.LUC
Diphtheria toxin i.p. (50 mg/kg x 2 days)
2W
3W
4W
5W
6W
7W
8W
C
Rostral
Dorsal
Caudal
Ventral
GFP/Hoechst
D
DT i.p.
BBB score
Time (wk)
GFP.LUC-NSC.VPA.DT, n = 9
TR6.GFP.LUC-NSC.VPA.DT, n = 6
TR6.GFP.LUC-NSC, n = 6
VPA, n = 8
No treatment, n = 8
E
DT i.p.
NMDA injection to spinal cord
BBB score
Time (wk)
GFP.LUC-NSC.VPA.DT, n = 4
GFP.LUC-NSC.VPA.DT.NMDA, n = 5
TR6.GFP.LUC-NSC.VPA.DT, n = 3
TR6.GFP.LUC-NSC.VPA.DT.NMDA, n = 3
TR6.GFP.LUC-NSC, n = 6
VPA, n = 8
No treatment, n = 5
No treatment.NMDA, n = 3

Figure 6
Ablation of transplanted cells abolishes hind limb motor function recovery. (**A**) Schematic of the protocols for NSC transplantation and for detection and ablation of transplanted cells. NSCs derived from GFP.LUC- or TR6.GFP.LUC-Tg mice were transplanted into SCI model mice 1 week after injury. VPA was intraperitoneally administered every day for 1 week. Survival of transplanted cells and locomotor function of the mice were monitored weekly for 14 weeks. (**B**) Survival of transplanted cells was checked every week using a bioluminescence imaging system. 6 weeks after injury (5 weeks after transplantation), each mouse received 2 DT administrations. By the following week, LUC activity had completely disappeared in mice transplanted with TR6.GFP.LUC-NSCs (lower panel). (**C**) Sagittal sections from SCI model mice transplanted with GFP.LUC- and TR6.GFP.LUC-NSCs 2 weeks after DT injection. All transplanted cells were ablated with DT (lower panel). Scale bar: 1 mm. (**D**) Time course of the changes in BBB scores in SCI model mice. The hind limb function of mice that had undergone dual treatment with TR6.GFP.LUC-NSCs and VPA dropped drastically after DT administration (black line). $^*P < 0.0001$ compared with GFP.LUC-NSC–transplanted, VPA-administered, and DT-injected SCI model mice (blue line) (repeated measures ANOVA). Data are mean ± SEM. VPA, $n = 8$; no treatment, $n = 8$. (**E**) Twelve weeks after injury, groups of SCI model mice received NMDA injections, as indicated, into the injury epicenter, to ablate local neurons in the gray matter (blue, black, and yellow lines with triangles). $^*P < 0.0001$ compared with non-NMDA–injected mice in each group (blue, black, and yellow lines with circles) (repeated measures ANOVA). Data represent mean ± SEM.

greater improvement compared with untreated mice (Figures 1 and 6). We suggest that, in severe SCI, supplementation with neurons may be more beneficial than supplementation with oligodendrocytes for reconstructing destroyed neuronal circuits. Our observation that transplant-derived neuronal axons could be remyelinated by endogenous oligodendrocytes (Supplemental Figure 9) suggests that the injured CNS may have a much greater restorative capacity than previously thought.

Differentiation of NSCs transplanted into the injured spinal cord is generally restricted to the glial lineage: the host spinal cord milieu is not permissive for neuronal differentiation (7, 21, 22, 47, 48). Neuronal differentiation of neuronal lineage–committed precursors grafted into the injured spinal cord is also severely inhibited, whereas the same cells can differentiate efficiently into neurons under in vitro culture conditions as well as in the intact spinal cord (47, 48). In an earlier attempt to stimulate neuronal differentiation, NSCs transduced with the proneural transcription factor neurogenin 2 (Neurog2) were engrafted into injured spinal cords, resulting in moderate functional recovery of hind limbs in comparison with untreated animals (11). The authors concluded, however, that oligodendrocytes derived unexpectedly from the transduced NSCs contributed to the improvement of motor function by remyelinating the injured axons. Although Neurog2-transduced NSCs actually differentiated more efficiently into neurons than into oligodendrocytes after transplantation, the roles of these neurons were not thoroughly investigated.

In the present study, we adopted what we believe is a novel approach for the treatment of SCI: manipulation of transplanted NSC fate by an epigenetic reagent. A combined treatment involving NSC transplantation and administration of the HDAC inhibitor VPA led to a marked functional recovery. We will refer below to this dual treatment as the HINT (HDAC inhibitor and NSC transplantation) method. Immunohistochemical analysis revealed that VPA administration promoted the neuronal differentiation of transplanted NSCs. We examined extensively the roles of the neurons responsible for reconstruction of broken neuronal networks using 2 neuronal tracers, immunoelectron microscopy, and 2 cell-ablation methods. These results revealed that transplant-derived neurons received projections from endogenous neurons and that their extended processes made synapses with endogenous neurons in the ventral horn. Furthermore, we showed clearly that transplant-derived neurons reconstructed the disrupted CST, allowing the restoration of signal transmission in a relay manner (Figure 7). Among these transplant-derived neurons, 16.9% ± 2.3% were vesicular glutamate transporter (VGLUT) 2-positive (glutamatergic) and 70.1% ± 1.8% were glutamic acid decarboxylase (GAD) 65 positive (GABAergic) (Supplemental Figure 10). Although we have not examined the neuronal subtypes of the remaining 13%, these data suggest that both excitatory and inhibitory neuronal subtypes were generated from transplanted NSCs. In light of these findings, we hypothesize that the balance between the transplant-derived excitatory and inhibitory neuronal subtypes is important for hind limb functional recovery after SCI. However, we must await further investigation to substantiate this hypothesis.

Although recovery was not as great as it was in mice that underwent the HINT method, mice treated with NSCs alone showed greater improvement of hind limb function compared with the untreated controls, which exhibited slight but significant restoration (Figures 1 and 6). This is probably due to trophic support provided by transplanted cells to endogenous cells, as suggested in previous reports (12–14), since transplanted NSCs barely differentiate into neurons in the injured spinal cord. However, any beneficial trophic effect of transplanted NSCs on endogenous neurons is unlikely to be sufficient to explain the functional recovery of the injured spinal cord because we did not observe axon reextension beyond the lesion site in our severe SCI model even in mice treated by the HINT method. Thus, it is likely that local neurons in the spinal cord (perhaps a mixture of preserved endogenous neurons and transplant-derived neurons) transmit signals in a relay manner. This is also supported by the fact that both spontaneous and treatment-provoked hind limb functional restoration were completely reversed by NMDA injection to ablate local neurons in the spinal cord (Figure 6E).

As an established drug for long-term therapy for epilepsy, VPA may be more appropriate for use in clinical trials than other drugs or ectopically expressed Tgs. Nonetheless, while the combination of epigenetic manipulation and NSC transplantation for the treatment of SCI yielded a dramatic functional improvement in hind limb movement, recovery was incomplete. To achieve a more efficient treatment for SCI, administration of a more complex "cocktail" (combinatorial treatment in conjunction with other strategies, such as neurotrophin-mediated prevention of neuronal death, regeneration of axons by suppressing myelin inhibitors, and remyelination) may be necessary.

Methods

Tg mice. For visualization and specific ablation of transplanted cells, we used the TRECK method (40). To achieve more specific and conditional ablation of target cells, we introduced 2 point mutations (I117V/L148V) in human *HB-EGF* (39). The modified human *HB-EGF* (*I117V/L148V*) gene fragment fused with *EGFP* was subcloned into *Eco*RI sites in the mammalian expression vector pCAGGS (49) (pCAG-TR6/GFP). The 3.8-kb *Spe*I-*Hin*dIII fragment was isolated from pCAG-TR6/GFP and microinjected into fertilized mouse eggs (C57BL/6J Jcl background). These eggs were

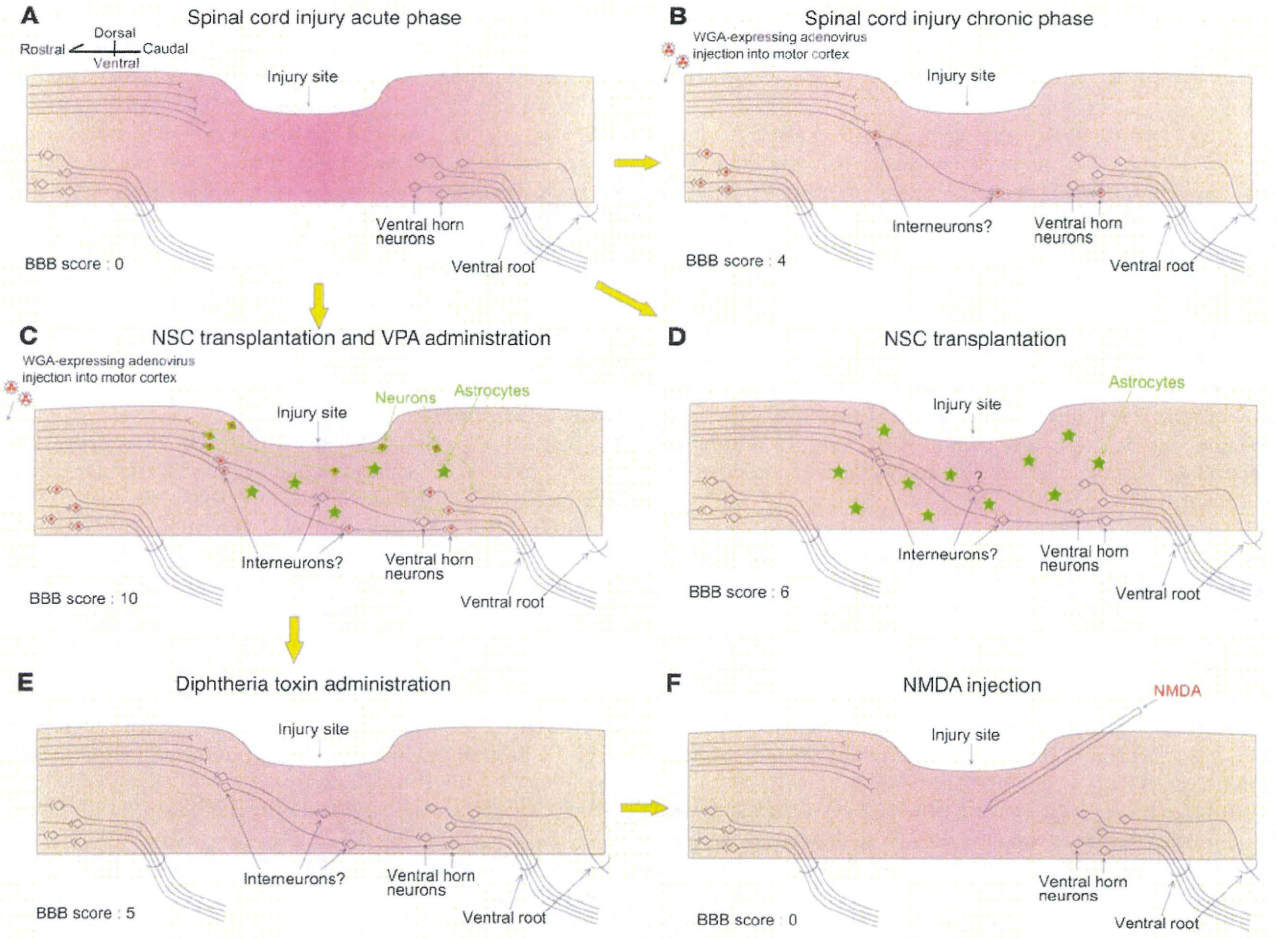

Figure 7

Diagrammatic summary of destruction and reconstruction of neural circuits in the injured spinal cord. (**A**) In the acute phase of SCI, CST fibers are disrupted and hind limb movement is completely lost. (**B**) In the chronic phase, WGA transport through the lesion site to the caudal area is negligible, probably because very few CST fibers are restored. (**D**) When NSCs were transplanted to the injured spinal cord, almost all of them differentiated into astrocytes, with the result that very little restoration of the injured CST occurred. (**C**) Following VPA administration, neuronal differentiation of transplanted NSCs was greatly enhanced and dramatic functional recovery could be observed. WGA is conveyed through the lesion site to the caudal area via transplant-derived neurons. (**E**) Ablation of transplant-derived cells with DT nullified hind limb functional recovery, suggesting that the transplanted cells contribute directly to the functional recovery in hind limbs. (**F**) Ablation of residual local neurons in the lesion site by NMDA led to a complete impairment of hind limb movement, suggesting that residual local endogenous neurons also play an important role in the improvement of hind limb motor function.

subsequently implanted into pseudopregnant female mice (C57BL/6J Jcl) to obtain the Tg mouse line TR6.GFP-Tg. Female mice homozygous for the CAG-LUC Tg (LUC-Tg) were mated with TR6.GFP-Tg heterozygous or CAG-GFP (GFP-Tg) (33) heterozygous male mice. E14.5 forebrain-derived NSCs from mice heterozygous for GFP (GFP-NSCs), TR6.GFP, and LUC (TR6.GFP.LUC-NSCs) or for GFP and LUC (GFP.LUC-NSCs) were expanded and used for transplantation. Tg mice expressing GFP under the control of the CAG promoter were a gift from M. Okabe (Osaka University, Suita, Osaka, Japan).

Cell culture. E14.5 mouse forebrains were dissected and triturated in calcium- and magnesium-free HBSS and cultured on poly-ornithine/fibronectin-coated (O/F-coated) dishes for 4 days in N2-supplemented DMEM/F-12 containing 10 ng/ml bFGF (PeproTech). Cells were replated on O/F-coated dishes in NS-A medium (Euroclone) supplemented with modified N2 and 10 ng/ml each of EGF (PeproTech) and bFGF (NS expansion medium) (36). We routinely used HBSS to detach cells from the dish; we split cells 1:3 and replated them onto O/F-coated dishes every 2 days. Cells that had been passaged 5–10 times were used for transplantation. See Supplemental Methods for details of NSC differentiation in vitro.

SCI model. All animal studies were conducted with the approval of the Nara Institute of Science and Technology animal care and use committee. We used 15-week-old male ICR mice weighing 37–45 g. Anesthetized (sodium pentobarbital, 40 mg/kg body weight) mice received laminectomies and partial laminectomies at the ninth and tenth thoracic spinal vertebrae, respectively. The dorsal surface of the dura mater was exposed and SCI was applied using an SCI device (90 kdyn; Infinite Horizon impactor; Precision Systems & Instrumentation) as previously described (8). The muscle and skin were closed in layers. The mice underwent manual bladder evacuation once a day. We checked the lesion site sizes in several SCI mice 1 week

after injury and confirmed that they were comparable. One week after the injury, hind limb movement in the model mice was not observed (BBB score: 0). Mice with incomplete injury (BBB score above 0 at 1 week after injury) were excluded (2.4%).

Transplantation. Seven days after injury, mice were anesthetized and transplanted with NSCs using a glass micropipette attached to a stereotaxic injector (Narishige). The tip of the micropipette was inserted into the injury epicenter in the injured spinal cord, and 2 μl of NS medium lacking growth factor, with or without NSCs (0.5×10^6/μl), was injected at a rate of 1 μl/min. All mice subcutaneously received cyclosporine immunosuppressant (10 mg/kg) and gentamicin (8 mg/kg) daily. After transplantation, mice were given daily intraperitoneal injections of VPA (150 mg/kg) or saline (control) for the following 7 days.

Behavioral testing. We evaluated the motor function of the hind limbs for up to 14 weeks after injury. See Supplemental Methods for details.

Immunocytochemistry. Immunocytochemical experiments were performed as described previously (7). See Supplemental Methods for antibodies used and further details.

Immunohistochemistry. We performed immunohistochemical analysis on tissue sections using 3 or more independent samples from the mice. See Supplemental Methods for details.

Immunoelectron microscopy. See Supplemental Methods.

Anterograde labeling of the CST. Twelve weeks after injury, descending CST fibers were labeled with BDA (10% in saline, 2 μl per cortex, MW 10,000; Molecular Probes) (6, 16, 17) by injection into the left and right motor cortices (50) (for 3 uninjured mice, 3 mice that received SCI with no treatment, and 3 mice that received SCI and underwent combined treatment with NSCs and VPA). See Supplemental Methods for details.

Visualization of multisynaptic neuronal pathways. To visualize selective and functional transsynaptic neuronal pathways, WGA-expressing recombinant adenoviruses (provided by Y. Yoshihara, RIKEN Brain Science Institute, Wako, Saitama, Japan) were used (38). In this system, injections of WGA-expressing adenovirus in well-mapped neural pathways result in labeling of first-, second-, and third-order neurons. WGA protein is efficiently transported in axons and dendrites in both anterograde and retrograde directions. See Supplemental Methods for details.

In vivo imaging of transplanted cells. In vivo imaging experiments were performed as described previously (8). See Supplemental Methods for details.

Ablation of transplant-derived cells. Cell ablation experiments were performed as described previously (39, 40). See Supplemental Methods for details.

Ablation of local neurons. To ablate neurons localized in the gray matter, NMDA was injected into the spinal cord at thoracic vertebrae 9 (Th9). Twelve weeks after injury, SCI model mice (5 GFP.LUC-NSC–transplanted and VPA-treated mice, 3 TR6.GFP.LUC-NSC–transplanted and VPA-treated mice, and 3 untreated mice) received bilateral injections of NMDA into 2 sites of the spinal cord (0.5 ml of 10 mM in saline per site) under anesthesia.

Statistics. We performed statistical analysis with an unpaired 2-tailed Student's *t* test for single comparisons. For analysis of the open-field scores, we used repeated measures ANOVA (Prism, GraphPad). $P < 0.05$ was considered significant.

Acknowledgments

We thank Y. Yoshihara for providing the WGA-expressing adenovirus and M. Okabe for donating the Tg mice expressing GFP under the control of the CAG promoter. We also thank Y. Bessho, T. Matsui, S. Komai, M. Arai, H. Fujioka, T. Yamashita, M. Ueno, Y. Sasai, K. Muguruma, B. Juliandi, K. Yone, T. Setoguchi, and Y. Fujimoto for valuable discussions and technical advice; I. Smith for editing the manuscript; and N. Ueda and M. Tano for secretarial assistance. This work was supported by the Naito Foundation, the NAIST Cross-Fields Collaboration Promoting Project, and by a grant-in-aid for Exploratory Research, a grant-in-aid for Young Scientists (B), and the NAIST Global COE Program (Frontier Biosciences: Strategies for Survival and Adaptation in a Changing Global Environment) from the Ministry of Education, Culture, Sports, Science, and Technology of Japan.

Received for publication March 11, 2010, and accepted in revised form July 7, 2010.

Address correspondence to: Kinichi Nakashima, Laboratory of Molecular Neuroscience, Graduate School of Biological Sciences, Nara Institute of Science and Technology, 8916-5 Takayama, Ikoma 631-0192, Japan. Phone: 81.743.72.5471; Fax: 81.743.72.5479; E-mail: kin@bs.naist.jp.

1. Thuret S, Moon LD, Gage FH. Therapeutic interventions after spinal cord injury. *Nat Rev Neurosci.* 2006;7(8):628–643.
2. David S, Aguayo AJ. Axonal elongation into peripheral nervous system "bridges" after central nervous system injury in adult rats. *Science.* 1981;214(4523):931–933.
3. Richardson PM, McGuinness UM, Aguayo AJ. Axons from CNS neurons regenerate into PNS grafts. *Nature.* 1980;284(5753):264–265.
4. Schnell L, Schwab ME. Axonal regeneration in the rat spinal cord produced by an antibody against myelin-associated neurite growth inhibitors. *Nature.* 1990;343(6255):269–272.
5. Bregman BS, Kunkel-Bagden E, Schnell L, Dai HN, Gao D, Schwab ME. Recovery from spinal cord injury mediated by antibodies to neurite growth inhibitors. *Nature.* 1995;378(6556):498–501.
6. Bradbury EJ, et al. Chondroitinase ABC promotes functional recovery after spinal cord injury. *Nature.* 2002;416(6881):636–640.
7. Setoguchi T, et al. Treatment of spinal cord injury by transplantation of fetal neural precursor cells engineered to express BMP inhibitor. *Exp Neurol.* 2004;189(1):33–44.
8. Okada S, et al. In vivo imaging of engrafted neural stem cells: its application in evaluating the optimal timing of transplantation for spinal cord injury. *Faseb J.* 2005;19(13):1839–1841.
9. Cummings BJ, et al. Human neural stem cells differentiate and promote locomotor recovery in spinal cord-injured mice. *Proc Natl Acad Sci U S A.* 2005;102(39):14069–14074.
10. Ogawa Y, et al. Transplantation of in vitro-expanded fetal neural progenitor cells results in neurogenesis and functional recovery after spinal cord contusion injury in adult rats. *J Neurosci Res.* 2002;69(6):925–933.
11. Hofstetter CP, et al. Allodynia limits the usefulness of intraspinal neural stem cell grafts; directed differentiation improves outcome. *Nat Neurosci.* 2005;8(3):346–353.
12. Shumsky JS, Tobias CA, Tumolo M, Long WD, Giszter SF, Murray M. Delayed transplantation of fibroblasts genetically modified to secrete BDNF and NT-3 into a spinal cord injury site is associated with limited recovery of function. *Exp Neurol.* 2003;184(1):114–130.
13. Tobias CA, et al. Delayed grafting of BDNF and NT-3 producing fibroblasts into the injured spinal cord stimulates sprouting, partially rescues axotomized red nucleus neurons from loss and atrophy, and provides limited regeneration. *Exp Neurol.* 2003;184(1):97–113.
14. Yan J, Welsh AM, Bora SH, Snyder EY, Koliatsos VE. Differentiation and tropic/trophic effects of exogenous neural precursors in the adult spinal cord. *J Comp Neurol.* 2004;480(1):101–114.
15. Keirstead HS, et al. Human embryonic stem cell-derived oligodendrocyte progenitor cell transplants remyelinate and restore locomotion after spinal cord injury. *J Neurosci.* 2005;25(19):4694–4705.
16. Hata K, et al. RGMa inhibition promotes axonal growth and recovery after spinal cord injury. *J Cell Biol.* 2006;173(1):47–58.
17. Kaneko S, et al. A selective Sema3A inhibitor enhances regenerative responses and functional recovery of the injured spinal cord. *Nat Med.* 2006;12(12):1380–1389.
18. Mi S, et al. LINGO-1 antagonist promotes spinal cord remyelination and axonal integrity in MOG-induced experimental autoimmune encephalomyelitis. *Nat Med.* 2007;13(10):1228–1233.
19. Nakamura M, Houghtling RA, MacArthur L, Bayer BM, Bregman BS. Differences in cytokine gene expression profile between acute and secondary injury in adult rat spinal cord. *Exp Neurol.* 2003;184(1):313–325.
20. Setoguchi T, et al. Traumatic injury-induced BMP7 expression in the adult rat spinal cord. *Brain Res.* 2001;921(1-2):219–225.

21. Martino G, Pluchino S. The therapeutic potential of neural stem cells. *Nat Rev Neurosci.* 2006; 7(5):395–406.
22. Abematsu M, Smith I, Nakashima K. Mechanisms of neural stem cell fate determination: extracellular cues and intracellular programs. *Curr Stem Cell Res Ther.* 2006;1(2):267–277.
23. Blaheta RA, Cinatl J Jr. Anti-tumor mechanisms of valproate: a novel role for an old drug. *Med Res Rev.* 2002;22(5):492–511.
24. Gottlicher M, et al. Valproic acid defines a novel class of HDAC inhibitors inducing differentiation of transformed cells. *Embo J.* 2001;20(24):6969–6978.
25. Phiel CJ, Zhang F, Huang EY, Guenther MG, Lazar MA, Klein PS. Histone deacetylase is a direct target of valproic acid, a potent anticonvulsant, mood stabilizer, and teratogen. *J Biol Chem.* 2001;276(39):36734–36741.
26. Hsieh J, Nakashima K, Kuwabara T, Mejia E, Gage FH. Histone deacetylase inhibition-mediated neuronal differentiation of multipotent adult neural progenitor cells. *Proc Natl Acad Sci U S A.* 2004;101(47):16659–16664.
27. Hashimoto R, Hough C, Nakazawa T, Yamamoto T, Chuang DM. Lithium protection against glutamate excitotoxicity in rat cerebral cortical neurons: involvement of NMDA receptor inhibition possibly by decreasing NR2B tyrosine phosphorylation. *J Neurochem.* 2002;80(4):589–597.
28. Kanai H, Sawa A, Chen RW, Leeds P, Chuang DM. Valproic acid inhibits histone deacetylase activity and suppresses excitotoxicity-induced GAPDH nuclear accumulation and apoptotic death in neurons. *Pharmacogenomics J.* 2004;4(5):336–344.
29. Ren M, Leng Y, Jeong M, Leeds PR, Chuang DM. Valproic acid reduces brain damage induced by transient focal cerebral ischemia in rats: potential roles of histone deacetylase inhibition and heat shock protein induction. *J Neurochem.* 2004;89(6):1358–1367.
30. Kim AJ, Shi Y, Austin RC, Werstuck GH. Valproate protects cells from ER stress-induced lipid accumulation and apoptosis by inhibiting glycogen synthase kinase-3. *J Cell Sci.* 2005;118(pt 1):89–99.
31. Peng GS, et al. Valproate pretreatment protects dopaminergic neurons from LPS-induced neurotoxicity in rat primary midbrain cultures: role of microglia. *Brain Res Mol Brain Res.* 2005;134(1):162–169.
32. Yuan PX, Huang LD, Jiang YM, Gutkind JS, Manji HK, Chen G. The mood stabilizer valproic acid activates mitogen-activated protein kinases and promotes neurite growth. *J Biol Chem.* 2001;276(34):31674–31683.
33. Okabe M, Ikawa M, Kominami K, Nakanishi T, Nishimune Y. 'Green mice' as a source of ubiquitous green cells. *FEBS Lett.* 1997;407(3):313–319.
34. Johe KK, Hazel TG, Muller T, Dugich-Djordjevic MM, McKay RD. Single factors direct the differentiation of stem cells from the fetal and adult central nervous system. *Genes Dev.* 1996;10(24):3129–3140.
35. Nakashima K, et al. Synergistic signaling in fetal brain by STAT3-Smad1 complex bridged by p300. *Science.* 1999;284(5413):479–482.
36. Conti L, et al. Niche-independent symmetrical self-renewal of a mammalian tissue stem cell. *PLoS Biol.* 2005;3(9):e283.
37. Basso DM, Beattie MS, Bresnahan JC. A sensitive and reliable locomotor rating scale for open field testing in rats. *J Neurotrauma.* 1995;12(1):1–21.
38. Kinoshita N, Mizuno T, Yoshihara Y. Adenovirus-mediated WGA gene delivery for transsynaptic labeling of mouse olfactory pathways. *Chem Senses.* 2002;27(3):215–223.
39. Furukawa N, Saito M, Hakoshima T, Kohno K. A diphtheria toxin receptor deficient in epidermal growth factor-like biological activity. *J Biochem.* 2006;140(6):831–841.
40. Saito M, et al. Diphtheria toxin receptor-mediated conditional and targeted cell ablation in transgenic mice. *Nat Biotechnol.* 2001;19(8):746–750.
41. Bareyre FM, Kerschensteiner M, Raineteau O, Mettenleiter TC, Weinmann O, Schwab ME. The injured spinal cord spontaneously forms a new intraspinal circuit in adult rats. *Nat Neurosci.* 2004;7(3):269–277.
42. Courtine G, et al. Recovery of supraspinal control of stepping via indirect propriospinal relay connections after spinal cord injury. *Nat Med.* 2008;14(1):69–74.
43. Faulkner JR, Herrmann JE, Woo MJ, Tansey KE, Doan NB, Sofroniew MV. Reactive astrocytes protect tissue and preserve function after spinal cord injury. *J Neurosci.* 2004;24(9):2143–2155.
44. Agrawal SK, Fehlings MG. Role of NMDA and non-NMDA ionotropic glutamate receptors in traumatic spinal cord axonal injury. *J Neurosci.* 1997;17(3):1055–1063.
45. Yu SP, Yeh C, Strasser U, Tian M, Choi DW. NMDA receptor-mediated K+ efflux and neuronal apoptosis. *Science.* 1999;284(5412):336–339.
46. Ditunno JF Jr, Formal CS. Chronic spinal cord injury. *N Engl J Med.* 1994;330(8):550–556.
47. Cao QL, Howard RM, Dennison JB, Whittemore SR. Differentiation of engrafted neuronal-restricted precursor cells is inhibited in the traumatically injured spinal cord. *Exp Neurol.* 2002;177(2):349–359.
48. Han SS, Kang DY, Mujtaba T, Rao MS, Fischer I. Grafted lineage-restricted precursors differentiate exclusively into neurons in the adult spinal cord. *Exp Neurol.* 2002;177(2):360–375.
49. Niwa H, Yamamura K, Miyazaki J. Efficient selection for high-expression transfectants with a novel eukaryotic vector. *Gene.* 1991;108(2):193–199.
50. Pronichev IV, Lenkov DN. Functional mapping of the motor cortex of the white mouse by a microstimulation method. *Neurosci Behav Physiol.* 1998;28(1):80–85.

BMP-induced REST regulates the establishment and maintenance of astrocytic identity

Jun Kohyama,[1] Tsukasa Sanosaka,[1] Akinori Tokunaga,[2] Eriko Takatsuka,[1] Keita Tsujimura,[1] Hideyuki Okano,[2] and Kinichi Nakashima[1]

[1]Laboratory of Molecular Neuroscience, Graduate School of Biological Sciences, Nara Institute of Science and Technology, Nara 630-0101, Japan
[2]Department of Physiology, Keio University School of Medicine, Tokyo 160-8582, Japan

Once they have differentiated, cells retain their individual character and repress genes that are specifically expressed in other cell lineages, but how alternative fate choice is restricted during and/or after differentiation remains unclear. In the mammalian central nervous system, neurons, astrocytes, and oligodendrocytes are generated throughout life from common tripotent neural progenitor cells (NPCs). Bone morphogenetic proteins (BMPs) are well-known astrocyte-inducing cytokines. We show here that the expression of a transcriptional repressor, RE1 silencer of transcription (REST)/neuron-restrictive silencer factor (NRSF), is up-regulated and sustained by BMP signal activation in the course of astrocytic differentiation of NPCs, and restricts neuronal differentiation. We further show that, in differentiated astrocytes, endogenous REST/NRSF associates with various neuronal genes and that disruption of its function resulted in their derepression, thereby explaining how ectopic neuronal gene expression is prevented in cells with astrocytic traits. Collectively, our results suggest that REST/NRSF functions as a molecular regulator of the nonneuronal phenotype in astrocytes.

Introduction

The mammalian cerebral cortex originates from neural progenitor cells (NPCs), which proliferate and give rise to the three major brain cell types: neurons, astrocytes, and oligodendrocytes (Gage, 2000; Temple, 2001). The fate of NPCs in the developing brain is believed to be determined by internal cellular programs and external cues that involve various types of cytokines (Gage, 2000; Schuurmans and Guillemot, 2002; Hsieh and Gage, 2004). Among the three NPC progeny types, mechanisms of differentiation have been most extensively investigated for astrocytes. The Janus kinase (JAK) signal transducer and activator of transcription (STAT) pathway (Bonni et al., 1997; Nakashima et al., 1999a; He et al., 2005) and the signaling pathway triggered by bone morphogenetic proteins (BMPs) are deeply involved in astrocytogenesis (Nakashima et al., 1999b; See et al., 2007). Despite considerable progress in unraveling how astrocytic traits are acquired, mechanisms that suppress differentiation into other cell lineages, such as neurons, during astrocytic specification remain poorly understood.

Neurogenesis is promoted by proneural basic helix-loop-helix (bHLH) transcriptional factors including Mash1 (mammalian achaete-scute homologue), Neurogenin, and NeuroD (mammalian atonal homologue), which form heterodimers with other ubiquitously expressed bHLH proteins such as the E2A gene products E12 and E47 (Bertrand et al., 2002). Consistent with their role in inducing neuronal differentiation, proneural factors are transiently expressed in neuronal progenitor cells located in the ventricular zone when neurogenesis is occurring in the developing central nervous system (CNS; Gradwohl et al., 1996; Tokunaga et al., 2004). The function of these proneural bHLH factors is inhibited by negative HLH proteins, such as the Id (inhibitor of differentiation) and Hes (hairy enhancer of split) families, at the onset of astroglial differentiation triggered by BMP2 (Nakashima et al., 2001). These findings partially explain cell fate decisions that facilitate the differentiation of one cell lineage and suppress that of the others: once NPCs are

Correspondence to Kinichi Nakashima: kin@bs.naist.jp

Abbreviations used in this paper: bHLH, basic helix-loop-helix; BMP, bone morphogenetic protein; ChIP, chromatin immunoprecipitation; CNS, central nervous system; DN, dominant negative; ES, embryonic stem; Hes, hairy enhancer of split; Id, inhibitor of differentiation; NPC, neural progenitor cell; NRSF, neuron-restrictive silencer factor; REST, RE1 silencer of transcription; SBE, Smad-binding element.

The Rockefeller University Press $30.00
J. Cell Biol.
www.jcb.org/cgi/doi/10.1083/jcb.200908048

Supplemental Material can be found at:
http://jcb.rupress.org/cgi/content/full/jcb.200908048/DC1

primed to differentiate into astrocytes, for example, neuronal differentiation must be inhibited. Although Id and Hes family members act by inhibiting proneural bHLH factors, thus preventing astrocytic lineage-committed NPCs from acquiring neuronal properties, their expression in vivo is generally observed in the proliferative zone, where undifferentiated but not differentiated cells reside (Duncan et al., 1992; Ellmeier and Weith, 1995; Lyden et al., 1999). Therefore, the ability to suppress neuronal properties in differentiated astrocytes should rely on regulatory pathway(s) downstream of Id and Hes, or on an as-yet-unidentified program which is subsequently established in differentiated astrocytes.

Insights into the mechanism that represses pan-neuronal gene expression in nonneural tissues have been gained from a series of studies regarding a zinc finger repressor protein, repressor element1-silencing transcription factor (REST)/neuron-restrictive silencer factor (NRSF) (Chong et al., 1995; Schoenherr et al., 1996; Chen et al., 1998; Lunyak et al., 2002; Conaco et al., 2006). The completion of neuronal differentiation is marked by the expression of proteins involved in electrophysiological processes, such as synapsin, glutamate receptors, SCG10, and type II sodium channel. Many other genes associated with the functional properties of terminally differentiated neurons have also been identified as direct targets of REST/NRSF (Bruce et al., 2004; Johnson et al., 2006; Otto et al., 2007). REST/NRSF suppresses target gene transcription through the association of its N- and C-terminal repressor domains with the mSin3/histone deacetylase-1/2(HDAC1/2) complex and with the CoREST complex, respectively (Huang et al., 1999; Lunyak et al., 2002). Suppression of neuronal gene expression by REST/NRSF is consistently observed in various cell types including PC12 cells (Ballas et al., 2001), myoblasts (Watanabe et al., 2004), and embryonic stem (ES) cells (Singh et al., 2008; Westbrook et al., 2008). Although several studies have suggested that REST/NRSF is a binary neuron/nonneuron fate regulator, its function has been examined mainly in nonneural cells and tissues. Concerning its role in the nervous system, REST/NRSF has been implicated in the acquisition of neuronal phenotype by NPCs in analyses of neuronal differentiation of ES cells (Ballas et al., 2005) and activation of REST/NRSF target genes induced by REST/NRSF-VP16 (in which the repressor domain is replaced with the activation domain of herpes simplex virus VP16; Su et al., 2004). In adult hippocampus-derived NPCs, REST/NRSF has been reported to promote neurogenesis through activation of its target genes by means of a small RNA-mediated functional switch that converts it from a suppressor to an activator of transcription (Kuwabara et al., 2004). Although these results strongly suggest the involvement of REST/NRSF in cell fate decisions of NPCs, it remains largely elusive how *REST/NRSF* expression is regulated in NPCs and how REST/NRSF participates in NPC fate specification and maintenance of the differentiated state of cells in the CNS.

In this study, we demonstrate that REST/NRSF is a critical suppressor of neuronal differentiation and neuronal gene expression during and/or after astroglial differentiation. The astrogliogenic cytokine BMP2 induced transcriptional activation of *REST/NRSF* in NPCs via the BMP-downstream transcription factor Smad, which binds to Smad-binding elements (SBEs) in the regulatory region of the *REST/NRSF* gene. Gain- and loss-of-function studies using wild-type REST/NRSF and a dominant-negative form of REST/NRSF (DN-REST/NRSF) in NPCs revealed a significant role for REST/NRSF in suppression of neuronal differentiation. Even in differentiated astrocytes, REST/NRSF continued to be expressed, and it associated with various neuronal genes containing the REST/NRSF binding site (RE1/NRSE). Furthermore, eliminating the repressor function of REST/NRSF led to derepression of neuronal genes in astrocytes, indicating that REST/NRSF acts to prevent astrocytes from displaying neuronal behavior.

Results

BMP2-induced expression of REST/NRSF in NPCs

As a first step to unraveling the mechanism by which neuronal gene expression is restricted in astrocytes, we hypothesized that the repression of neuronal character in astrocytes is programmed during a fate-determination step toward astrocytes. As shown in a previous study (Nakashima et al., 2001), BMP2 inhibited neuronal differentiation of NPCs (Fig. 1 A). BMP signal activation in NPCs was confirmed by detecting phosphorylation of Smads in response to BMP stimulation (Fig. S1 A). The frequency of Map2ab-positive neurons generated from NPCs on d 4 in BMP2-treated and untreated cultures was 3.7 ± 2.0% and 11.0 ± 3.7%, respectively. We also observed a reduction in the number of NPC- and oligodendrocyte-marker–positive cells by BMP2 treatment, suggesting that BMP2 inhibits differentiation of NPCs toward nonastrocytic lineages (Fig. S1, B and C). BMP2 induced the expression of negative HLH factor genes including *Id1*, *Id3*, and *Hes5* (Nakashima et al., 2001), whose products are known to inhibit neurogenic bHLH factors such as Neurogenin and Mash1. Although Ids and Hes5 thus seem to be candidate repressors of neuronal traits in differentiated astrocytes, their BMP-induced expression was transient, and they were not highly expressed in differentiated astrocytes (Nakashima et al., 2001; Fig. S1, D and E). Therefore, we set out to identify another candidate gene whose expression, in contrast to the Ids and Hes5, is induced by BMP2 and sustained. Among various transcriptional repressors, we focused on REST/NRSF because it is known as a repressor of neuronal gene expression in nonneural tissues, and found that REST/NRSF expression is indeed up-regulated by BMP2 treatment of NPCs (Fig. 1 B). Sustained REST/NRSF expression in BMP2-treated NPCs was further confirmed by Western blot (Fig. 1 C) and quantitative RT-PCR analysis (Fig. S1 E). As well as acting as a transcriptional repressor for neuronal genes, REST/NRSF is also a latent transcriptional activator in the adult CNS (Kuwabara et al., 2004). To monitor REST/NRSF function under our experimental conditions, we exploited a reporter construct carrying RE1/NRSE, a binding motif for REST/NRSF, fused upstream of an SV40 minimal promoter (Fig. 1 D, top). When this RE1/NRSE reporter was introduced into NPCs, luciferase reporter activity decreased in response to BMP2 treatment (Fig. 1 D, bottom left). On the other hand, we found no

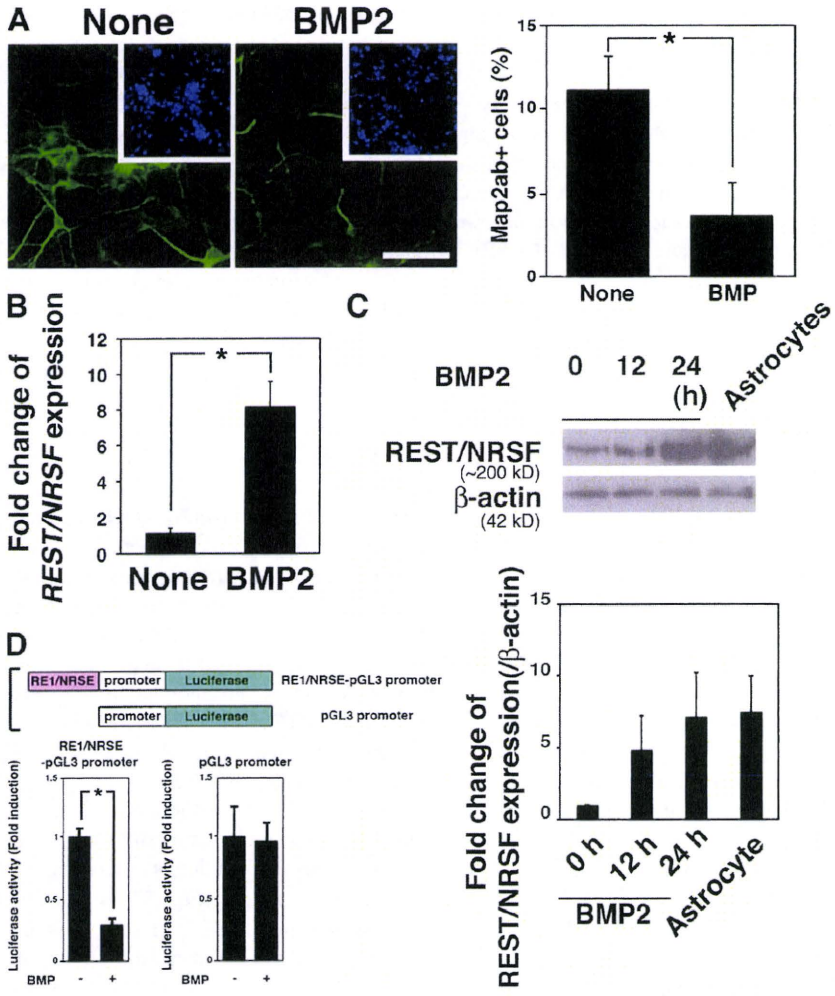

Figure 1. **BMP2 induces expression of *REST/NRSF*.** (A) NPCs were cultured for 4 d with or without BMP2 (50 ng/ml) in the presence of bFGF (10 ng/ml), and then immunostained for Map2ab (green). Inset (blue), Hoechst nuclear staining of each field. Percentages of Map2ab-positive cells were quantified (right; mean ± SD; $n = 3$). Statistical significance was examined by Student's t test (*, $P < 0.05$). (B) Total RNAs were extracted from NPCs treated or untreated with BMP2 (50 ng/ml) for 1 h and then subjected to quantitative RT-PCR using primer sets for *REST/NRSF* and *G3PDH* to evaluate expression of *REST/NRSF* mRNA. Statistical significance was examined by Student's t test (*, $P < 0.05$). (C) NPCs were treated with BMP2 (50 ng/ml) for 12 and 24 h. The cells were lysed for Western blot analysis to detect expression of REST/NRSF (~220 kD). Cell lysate from primary astrocytes from P0 mouse brain was used as a control. Fold change of REST/NRSF protein expression was analyzed by ImageJ software. (D) Schematic diagram of the construct to examine REST/NRSF activity. The RE1/NRSE element was fused upstream of the SV40 minimal promoter (top). NPCs were cotransfected with each reporter construct and pRL-CMV, and then stimulated with BMP2. After 48 h, luciferase activity was measured.

difference between control reporter activity with or without BMP2 treatment (Fig. 1 D, bottom right). Thus, these data suggest that REST/NRSF induced by BMP2 appears to function as a transcriptional repressor in embryonic NPCs.

REST/NRSF is a direct target of the BMP-Smad pathway

Having observed REST/NRSF up-regulation by BMP2 in NPCs, we next sought to gain mechanistic insight into BMP2-induced expression of REST/NRSF. The genomic structure of *REST/NRSF* has been extensively examined in previous studies (Koenigsberger et al., 2000; Kojima et al., 2001), and we identified two possible BMP-responsive SBEs (GCCGNCGC; Kusanagi et al., 2000), which are highly conserved between mouse and human, in the regulatory region of the gene (+1192 to +1199, and +1204 to +1211; Fig. 2 A). Next, we isolated a genomic fragment that contains the 5′ UTR of the mouse *REST/NRSF* gene, including the SBEs, to generate *REST/NRSF* reporter constructs. The intact reporter was activated by the expression of constitutively active BMP type I receptor (ALK3(QD); Imamura et al., 1997; Fig. 2 B), and this transactivation was severely compromised by mutating the two SBEs (Fig. 2 B). BMP2 activates Smad1, 5, and 8, and the activation is suppressed by the inhibitory Smad, Smad6 (Imamura et al., 1997). As shown in Fig. 2 C, transactivation of the *REST/NRSF* reporter by BMP signaling was inhibited by the expression of Smad6, and the same was true when a dominant-negative (DN) form of Smad1 (Yoshiura et al., 2007) was used instead of Smad6 (Fig. S2 A). These data, thus, suggest that activation of Smad1/5/8 is required for the induction of *REST/NRSF* gene expression. To determine whether Smads indeed bind to the SBE-containing endogenous *REST/NRSF* gene regulatory region after BMP2 stimulation, we performed a chromatin immunoprecipitation (ChIP) assay using anti-Smad1. As shown in Fig. 2 D, significant Smad binding to the SBE-containing fragment occurred in BMP2-treated cells. Collectively, these results suggest that *REST/NRSF* is a direct target of BMP signaling in NPCs. Although one could imagine that the sustained expression of *REST/NRSF* in astrocytes is established by permanent recruitment of Smads on its regulatory region, Smad1-enrichment to the region, which is induced in NPCs by BMP2 stimulation, was not observed in differentiated astrocytes, as judged by the ChIP assay (Fig. S2 B). Alternatively, we found that the regulatory region was marked by transcriptionally active histone